

Review

Structural, Morphological and Optical Properties of MoS₂-Based Materials for Photocatalytic Degradation of Organic Dye

Jadan Resnik Jaleel UC ¹, Madhushree R ¹, Sunaja Devi K R ^{1,*}, Dephan Pinheiro ¹ and Mothi Krishna Mohan ²¹ Department of Chemistry, CHRIST (Deemed to be University), Bangalore 560029, India² Department of Sciences and Humanities, School of Engineering and Technology, CHRIST (Deemed to be University), Kumbalagodu, Mysore Road, Bangalore 560074, India

* Correspondence: sunajadevi.kr@christuniversity.in

Abstract: Molybdenum disulfide (MoS₂) is a transition metal dichalcogenide (TMDCs) having versatile properties and plays a great role in the photodegradation of organic dyes. MoS₂ also finds applications in diverse fields such as catalysis, electronics, and nanomedicine transportation. MoS₂ can be prepared by using chemical and physical methods such as hydrothermal, solvothermal, and chemical vapour deposition methods. The preparation method employed can produce subtle but significant changes in the morphology. To increase the efficiency of MoS₂, it can be combined with different materials to produce composites that improve the photodegradation efficiency of MoS₂. The various methods of preparation, the morphology of MoS₂, and photodegradation activity of the MoS₂-based nanocomposites are briefly discussed in this review.

Keywords: MoS₂ nanomaterial; photocatalysis; dye degradation; nanocomposites



Citation: Jaleel UC, J.R.; R, M.; Devi K R, S.; Pinheiro, D.; Mohan, M.K. Structural, Morphological and Optical Properties of MoS₂-Based Materials for Photocatalytic Degradation of Organic Dye. *Photochem* **2022**, *2*, 628–650. <https://doi.org/10.3390/photochem2030042>

Academic Editors: Chuanyi Wang, Wanhong Ma, Myong Yong Choi, Jayaraman Theerthagiri and Seung Jun Lee

Received: 4 July 2022

Accepted: 4 August 2022

Published: 8 August 2022

Publisher's Note: MDPI stays neutral with regard to jurisdictional claims in published maps and institutional affiliations.



Copyright: © 2022 by the authors. Licensee MDPI, Basel, Switzerland. This article is an open access article distributed under the terms and conditions of the Creative Commons Attribution (CC BY) license (<https://creativecommons.org/licenses/by/4.0/>).

1. Introduction

The discovery of Buckminster fullerene (C₆₀) and carbon nanotubes (CNTs) in the late twentieth century marked a pivotal moment in nanomaterial research. These materials have since become a substitute for carbon-based bulk materials such as graphite and diamond. These materials have already made their presence felt and proved their utility in diverse fields [1]. A significant amount of studies have been done on the carbon nanotube as a versatile material in electronics and numerous other fields [2]. However, the inherent drawbacks in carbon nanotubes led to the discovery of materials like graphene [3], two-dimensional transition metal dichalcogenides (TMDCs), etc. The TMDCs are composed of a transition metal element (M) and chalcogen element (X) like S, Se, Te, etc. [4]. The layers are held together by the weak van der Waals forces. MoS₂ is a TMDCs having single-layer/monolayer or nanolayers formed from bulk material via exfoliation. [5]. There are about 40 different types of TMDCs [6], such as WSe₂, MoS₂, WS₂, etc. They are prepared by sandwiching a layer of transition metal (e.g., molybdenum, tungsten, niobium) atoms between two layers of chalcogen (e.g., sulphur, selenium, tellurium) atoms. MoS₂ is three atoms thick with a structure comprising of (X-M-X) S-Mo-S [7,8]. There are four different polytypes of MoS₂, namely, 1T, 1H, 2H, and 3R. These are classified based on the coordination of Mo atom and stacking orientation of the single layers [6]. MoS₂ has found extensive applications in photocatalysis and electrocatalysis [9,10]. MoS₂ and MoS₂-based nanomaterials have attracted a lot of attention for their high charge carrier potency and superb optical absorption property [11,12]. For commercial photocatalysis applications, a stable, efficient, and low-cost photocatalyst with a light-harvesting spectrum spanning the entire solar spectrum is highly desirable [13]. Photocatalytic materials can transform sunlight into chemical energy and use this to degrade organic pollutants into non-toxic carbon dioxide and tiny inorganic molecules like water without causing secondary pollution [14].

The poor interactions between the layers enable the formation of bulk equivalents of multi-layered materials, which support the stability of the structure. The interesting properties of TMDCs such as tuneable band gap ranging between 0–3 eV, high surface-to-volume ratio, semiconductor property, and the high availability of active sites on the surface have led to a wide range of applications such as gas sensing, optoelectronics, catalysis, energy storage, etc. [15]. The physical properties of these materials are amenable to alteration by inter-lamellar space intercalating or doping [5]. MoS₂ has a role in many fields such as catalysis, electronics [16–18], and nanomedicine transportation [19]. g-C₃N₄ is another material frequently utilized to alter the characteristics of MoS₂ in order to boost its catalytic efficiency [20].

The characteristics of single-layered MoS₂ differ significantly from those of their bulk counterparts. The large surface energy in MoS₂ makes it prone to aggregation, which can adversely impact its stability and efficiency as a catalyst [21,22]. This can be a serious drawback when MoS₂-based catalysts are used in the aqueous phase. This can be overcome by embedding MoS₂ within layered materials to achieve benefits to both materials, and improved performances can be realized [23,24]. MoS₂ is a photocatalyst for hydrogen evolution because it has a strong conductivity, wide basic surface region, sufficient band edge, solid lattice fit, and relatively high mobility. Layered MoS₂ is thought to be a good candidate for pairing with g-C₃N₄ because of its p-type conductivity. g-C₃N₄ is also an important photocatalytic substance for fuel generation from sunlight via water splitting and environmental remediation via organic pollutant degradation. ZnO, and CdS, which are also effective photocatalysts, have been used to alter the MoS₂ catalyst to improve its photocatalytic efficiency. In recent studies, MoS₂ has been widely explored in fields other than photocatalytic degradation. One major application that was studied is towards H₂ production [25]. MoS₂/Ni₃S₂/reduced graphene oxide electrocatalyst was studied for alcohol fuel cells [26], and on bacterial wound treatment [27]. The bacterial capturing and deactivating using MoS₂-based nanocomposites have also been studied.

Access to clean freshwater is a necessity for all human beings and, to a large extent, determines the quality of our lives. Pollution of the water bodies, particularly with industrial wastewater containing a variety of organic and inorganic pollutants, is an environmental issue worldwide [28]. According to the 2017 United Nations World Water Development report, 80% of wastewater is dumped into the environment without proper treatment [29]. The availability of various pollutants in water has serious health consequences for human health as well [30]. Further, the exploding population has placed an additional pressure on our diminishing freshwater resources [31]. Rapid industrialization and increasing agricultural activities have led to the generation of a large amount of wastewater [32]. Pollution of water also has adverse effects on the aquatic ecosystem. There is an urgent need to address this sorry state of affairs. Remediating wastewater through economic and eco-friendly protocols needs to be devised. One such technology for wastewater remediation is photocatalysis, which makes use of freely accessible sunlight to fuel the breakdown of organic contaminants present in wastewater [33]. Photocatalysis has risen in popularity in recent years because of its huge potential for resolving the growing energy crisis and environmental pollution. At moderate temperatures, solvothermal techniques can produce acceptable yields with varied controllability in the size of nanomaterials, which are successfully used in a variety of semiconductor applications [34].

This article briefly discusses the structure, geometry, methods of preparation, characterization, and application of MoS₂-based nanomaterials. The research achievements made in improving the degradation performance of MoS₂-based photocatalysts have been explored. The schematic illustration of the MoS₂-based catalysts' preparation, morphology, and applications are given in Figure 1.

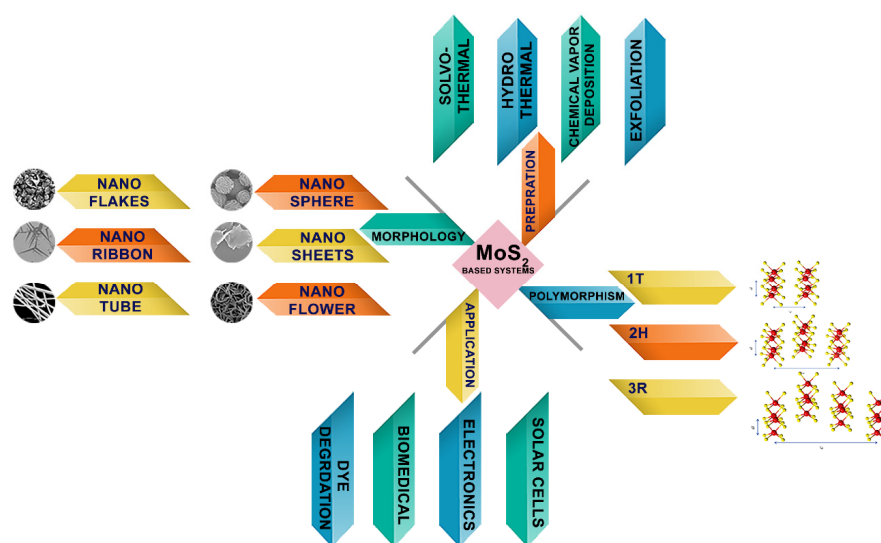


Figure 1. Representation of the preparation, morphology, and applications of MoS₂-based catalysts.

2. Structure and Geometries of MoS₂

MoS₂ is a black-coloured substance, insoluble in water, and like graphene, has a layered structure. It is mostly found in nature in the form of molybdenite. MoS₂ has excellent thermal and chemical stability, which is a feature of layered transition metal compounds in general. As a result, it is employed in nanochemistry, catalysis, electrode materials, pharmaceuticals, nanomedical transportation, etc. MoS₂ is a typical n-type semiconductor with a layered structure that is quite similar to graphene. The band gap of MoS₂ grows as the number of the atomic layers decreases, resulting in desirable photoelectric characteristics. MoS₂ is a stable 2D transition metal dichalcogenide, which means it is a semiconductor of the MX₂ type, where M stands for transition metals and X is for chalcogen [29]. A single sheet is similar to a “sandwich” structure, where the Mo atom is sandwiched between two S atoms [35,36]. MoS₂ layers, separated by 0.65 nm, are held together by van der Waals forces, and the layers are bound together by strong covalent bonds [37]. Figure 2a,b show the crystal structure of MoS₂ [16,38,39].

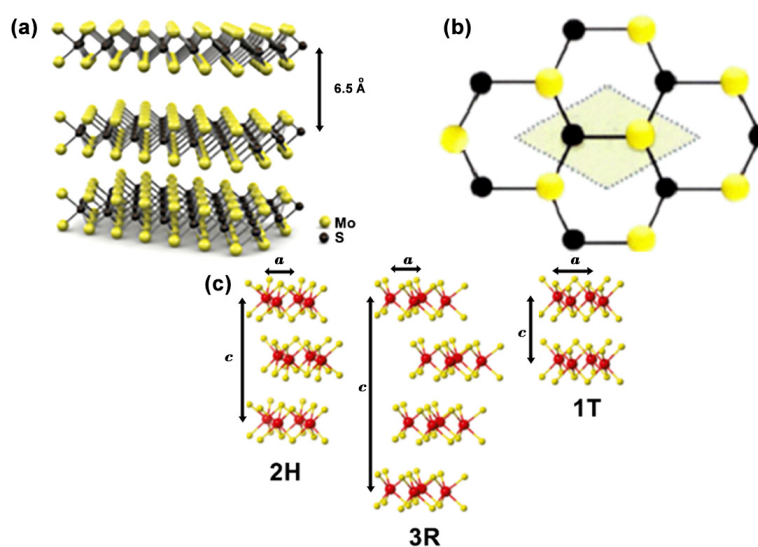


Figure 2. (a) Lateral view [16], (b) vertical view [38] of MoS₂ crystal structure, and (c) Crystal structure of MoS₂, 2H (left), 3R (centre), and 1T (right), respectively. Atom colour: Red-Mo, yellow-S [39]. Reprinted with permission from ref. [16,38,39]. Copyright 2011-Nature research, Copyright 2021-Elsevier, and Copyright 2016-Cell press.

MoS₂ is polytypic [4], with three distinct configurations: 1T [40], 2H [41], and 3R [42], all of which belong to symmetric point groups D_{6h}, D_{6d}, and C_{3v}, respectively [13]. The polymorphic structures are given in Figure 2c. The first digit in these polytypes denotes the number of layers in the make-up, while the alphabet denotes the crystallographic configuration. In these polytypes, the letters T, H, and R stand for trigonal, hexagonal, and rhombohedral arrangements. Various allotropes and morphologies, such as 3D (flowers, snowflakes, and dandelion patterns), 2D (nanosheets, nanostrips, and nanoribbons structure), 1D (nanowires and nanorods arrangement), and 0D (nanowires and nanorods) can be visualized, designed, and achieved by suitably altering the synthesis process. MoS₂ is a naturally occurring 2H molecule with 3% 3R that is thermodynamically stable.

MoS₂ monolayers show less activity in catalysis due to the limited charge mobility and a lack of metal edge sites. Increasing the number of exposed edge sites and using monolayered MoS₂ sheets having greater electrical conductivity have both improved the catalytic performances of MoS₂. However, the bulk of the metal on the basal plane of the monolayers still shows a lower catalytic activity [43]. From the studies conducted, it is evident that while the basal planes of 2H-MoS₂ are catalytically inert, the sulphur edge sites, and vacancy defects are the active sites for dye degradation. The photocatalytic dye degradation shows an enhancement when the size of the 2H-MoS₂ particles has been decreased to produce a higher density of edge sites. Another method for improving the catalytic activity of MoS₂ is to alter the 2H crystal phase to produce a polymorph with improved electrical conductivity, which will facilitate the transport of electrons to the active sites [44,45]. As stated below, MoS₂ comes in a variety of crystalline forms. The images given below are from the Materials projects database [46].

Hexagonal: The hexagonal structure of the MoS₂ is given in Figure 3. The structure of *P6₃/mmc* space group is given the Figure 3a. It shows a band gap of 1.465 eV and a density of 4.05 g/cm³. Lattice parameters of the structure are a = b = 3.190 Å, and c = 14.879 Å. $\alpha = \beta = 90^\circ$ $\gamma = 120^\circ$ and volume is 131.151 Å³. The structure of *P6m2* is given in Figure 3b. It has a band gap of 1.661 eV and a density of 2.80 g/cm³. Lattice parameters of the structure are a = b = 3.190 Å and c = 17.440 Å. $\alpha = \beta = 90^\circ$ $\gamma = 120^\circ$ and volume is 153.721 Å³ [46].

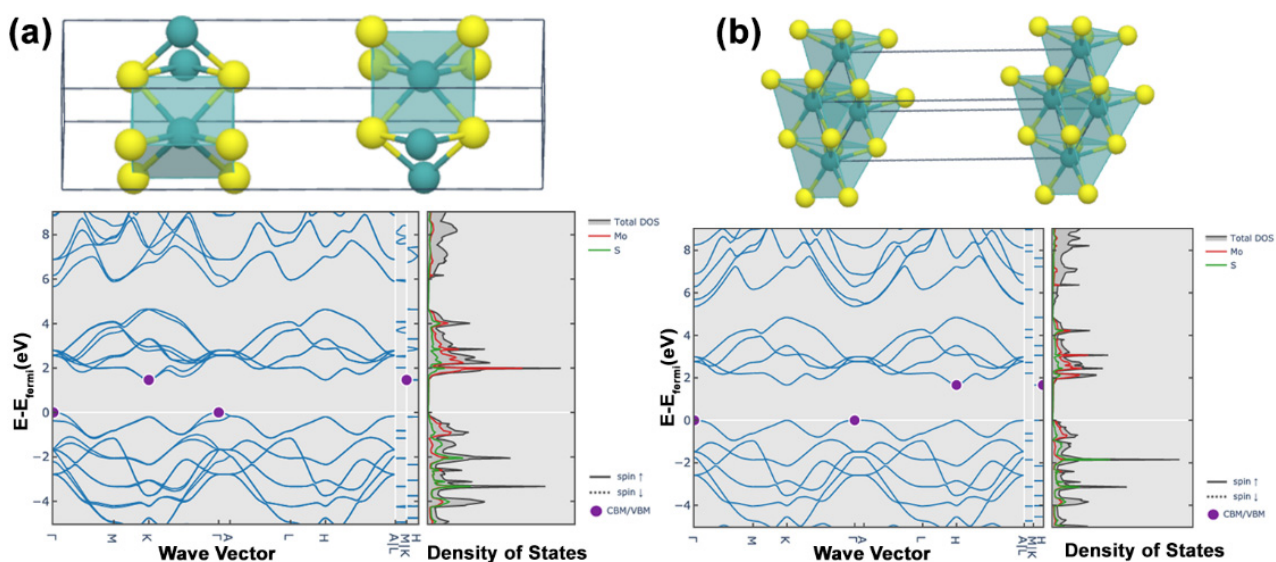


Figure 3. The geometrical representation of Hexagonal MoS₂ with their band structure and density of states of space group (a) *P6₃/mmc*, (b) *P6m2*. Reprinted with Creative Commons Attribution 4.0 License (CC BY 4.0) [46]. This work is licensed under copyleft, a CC BY 4.0 open source license.

Trigonal: The trigonal structure of the MoS₂ is given in Figure 4. The structure of the *R3m* space group is given in Figure 4a. It shows a band gap of 1.578 eV and a density of 4.24 g/cm³. Lattice parameters of the structure are $a = b = c = 7.341 \text{ \AA}$. $\alpha = \beta = \gamma = 25.103^\circ$, and volume is 62.649 \AA^3 . The structure of MoS₂ with the *P3m1* space group is given in Figure 4b. It shows a band gap of 1.554 eV and a density of 2.42 g/cm³. Lattice parameters of the structure are $a = b = 3.190 \text{ c} = 24.879 \text{ \AA}$. $\alpha = \beta = 90^\circ \gamma = 120^\circ$. Volume is 131.151 \AA^3 . The structure of the *P6m2* space group is given in Figure 4c, having a band gap of 1.509 eV and a density of 2.8 g/cm³. Lattice parameters of the structure are $a = b = 3.190 \text{ c} = 32.319 \text{ \AA}$. $\alpha = \beta = 90^\circ \gamma = 120^\circ$ and volume is 284.872 \AA^3 .

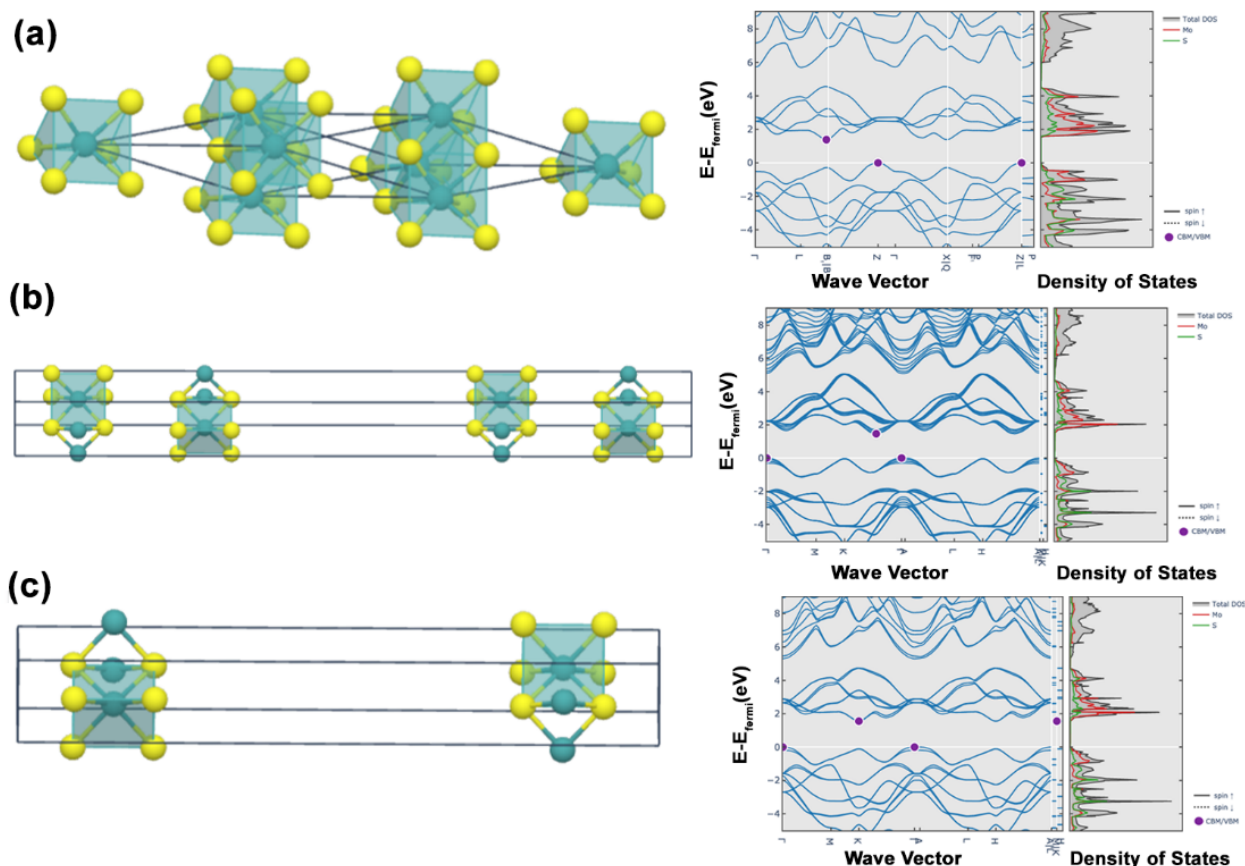


Figure 4. The geometrical representation of trigonal MoS₂ with their band structure and density of states of space group (a) *R3m*, (b) *P3m1*, (c) *P6m2*. Reprinted with Creative Commons Attribution 4.0 License (CC BY 4.0) [46]. This work is licensed under a copyleft CC BY 4.0 open source license.

Other geometries: The orthorhombic structure of the MoS₂ is given in Figure 5a. It has a band gap of 1.578 eV and a density of 2.67 g/cm³. The structure belongs to the *Pmnn* space group. Lattice parameters of the structure are $a = 3.163 \text{ b} = 13.021 \text{ c} = 43.774 \text{ \AA}$. $\alpha = \beta = \gamma = 90^\circ$, volume = 1790.583 \AA^3 . Figure 5b represents the cubic geometry of MoS₂. This structure has a band gap of 1.562 eV and a density of 4.81 g/cm³. The structure belongs to the *F43m* space group. Lattice parameters of the structure are $a = b = c = 6.778 \text{ \AA}$. $\alpha = \beta = \gamma = 60^\circ$, and volume = 221.129 \AA^3 . Figure 5c represents the tetragonal structure of MoS₂, and it has a band gap of 1.785 eV and a density of 3.27 g/cm³. The structure belongs to the *I42d* space group. Lattice parameters of the above structure are $a = b = c = 6.505 \text{ \AA}$. $\alpha = \beta = 128.852^\circ, \gamma = 75.248^\circ$, and volume = 162.514 \AA^3 [46].

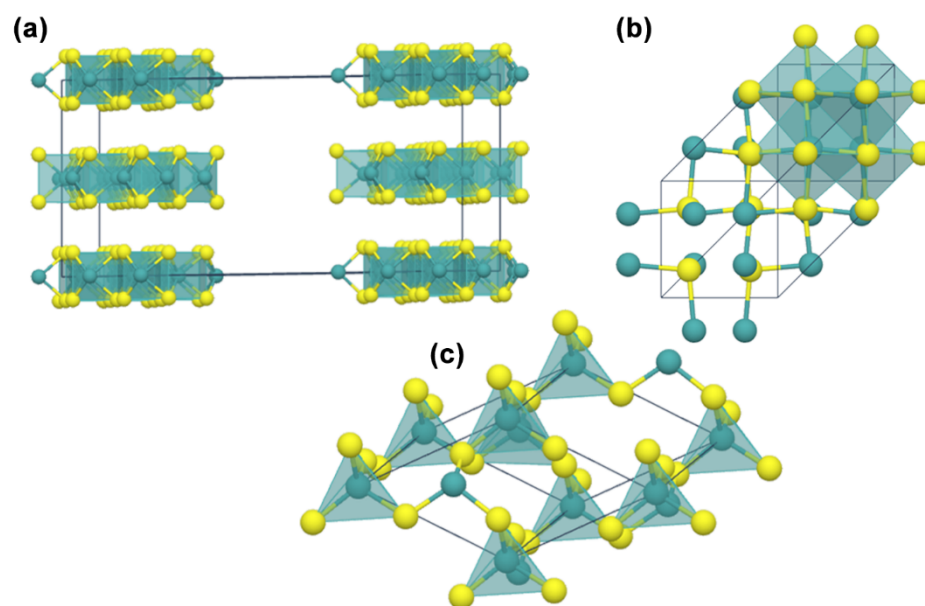


Figure 5. The geometrical representation of (a) Orthorhombic, (b) Cubic, (c) Tetragonal MoS₂. Reprinted with Creative Commons Attribution 4.0 License (CC BY 4.0) [46]. This work is licensed under a copyleft CC BY 4.0 opensource license.

3. Different Methods of Preparation of MoS₂

For the preparation of MoS₂, a variety of physical and chemical approaches have been used. The generally used physical methods are (a) mechanical exfoliation, (b) sputtering, (c) epitaxy, (d) plasma, etc. The lattice structure of the material will not change or be destroyed in this method, provided the precursor materials are pure [38]. However, in recent studies, physical methods are not commonly used since they are not cost effective. The chemical methods include (a) chemical vapor deposition method, (b) hydrothermal method, and (c) solvothermal method. The most common methods of preparation are listed in Figure 6.



Figure 6. Different methods of preparation of MoS₂-based systems.

3.1. Physical Methods

Mechanical exfoliation: Mechanical exfoliation is an approach used in the preparation of 2D materials, similar to the method used in monolayer graphene. Yu et al., developed a simple, environmentally friendly, and scalable exfoliation approach for water-dispersible

MoS₂ [47]. In the pre-treatment of MoS₂ powder, no intercalation agents have been used. Then, dispersion took place in ultrasound-assisted water—a typical exfoliation process for nanosheets—in combination with viscoelastic stinging for the preparation of MoS₂. Funke et al. used an micromechanical exfoliation method where they did not find any evident grid defects in elliptic-polarization spectra imaging [48]. This method is useful to manage the materials' surface and mechanical exfoliation. One drawback here is that the thickness and transverse dimensions are difficult to regulate and, therefore, the procedure is unsatisfactory and unsuitable for commercial manufacturing [49].

3.2. Chemical Methods

The chemical vapor deposition (CVD) method: This method can be used to prepare MoS₂ and transition metal dichalcogenides of high quality on a large scale, mainly to make MoS₂ films [50,51]. It is a bottom-up approach that preserves the defects, crystallinity, and morphology of the material [52]. CVD is a large-scale chemical reaction that involves vapors reacting with the substrate to produce thin films. Direct evaporation is used in the CVD process, commonly known as the vapour solid development technique. It creates a high-quality monolayer with fewer tiny flakes on the substrate. Precursors are charged and sublimated into a gaseous state which helps to undergo chemical reactions at high temperatures. Strong sediments grow on the matrix surface during condensation; hence it is commonly used to prepare monolayer nanocomposite systems and multilayer transition metal MoS₂ with good control on the number of layers.

MoO₃ powder is used as a molybdenum source and S powder as a sulfur source in the preparation of large-area monolayer MoS₂ films. Monolayer films grow consistently with a uniform nature, but defects created during the growth process cause a reduction in the material consistency [53]. In the preparation, improvements were made by Zhang et al., who produced triangular monolayers of MoS₂ with grain sizes up to 150 μm [54]. Alharbi et al. used a chemical vapor deposition process to create a large-area MoS₂ film with the highest island density in the field [55]. Balendhran et al. developed a two-step bulk fabrication technique using an MoO₃ precursor [56]. In a quartz channel, MoO₃ is evaporated on every substrate, followed by sulfidation. A schematic representation of synthesizing MoS₂ using the chemical vapour method and CVD growth of the MoS₂ when Mo foil is used as a precursor is depicted in Figure 7a,b, respectively [57,58].

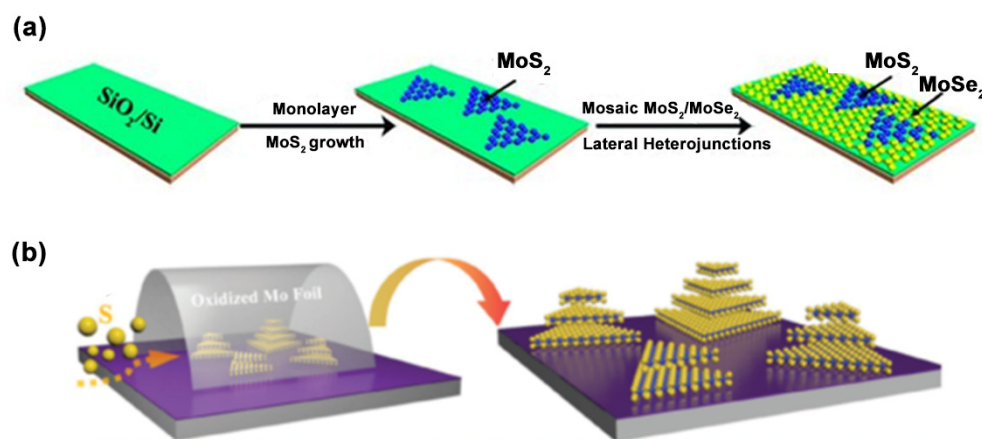


Figure 7. (a) Representation diagram of the synthesis of MoS₂ by chemical vapor deposition method [57] (b) Representation for the CVD growth of MoS₂ using arched oxidized Mo foil as the precursor [58]. Reprinted with permission from ref. [57,58]. Copyright 2018-MDPI, Copyright 2020-Elsevier.

Hydrothermal method: The hydrothermal method is a promising wet chemical method that is performed using a hydrothermal bomb. The temperature used for this method is usually 180 °C [59]. Typically, the precursors used are sodium molybdate

($\text{Na}_2\text{MoO}_4 \cdot 2\text{H}_2\text{O}$) and ammonium molybdate tetrahydrate ($(\text{NH}_4)_6\text{Mo}_7\text{O}_{24} \cdot 4\text{H}_2\text{O}$) for molybdenum and thiourea ($\text{CS}(\text{NH}_2)_2$) for sulfur. Nanosheets [60], nanospheres [61], nanoflowers [62], and nanotubes [63] can be prepared using hydrothermal methods. It is the most frequently used method for synthesis of flower-like MoS_2 [64]. Figure 8 represents the preparation steps of MoS_2 nanosheets. The molybdenum source was $\text{Na}_2\text{MoO}_4 \cdot 2\text{H}_2\text{O}$, and the sulfur source was thiourea in the synthesis proposed by Zou et al. [65]. The MoS_2 -RGO-3 was generated using a hydrothermal process and had a structure that resembles a cabbage, with distinct lattice fringes and a diameter range of 500 nm^{-1} . 3D MoS_2 ultrastructure was prepared by Anwer et al. [66], who used a controllable hydrothermal approach to achieve their results. These micro-sized marigold flower-like patterns were made up of 2D ultrathin MoS_2 nanosheets that were randomly spaced but closely connected. Controlling the input concentrations of thiourea and the precursor of MoS_2 resulted in the MoS_2 -microflower composition. Tong et al. [67] have used a previously published hydrothermal method for MoS_2 preparation. The flower-like MoS_2 had a hierarchical structure with a diameter of 500 nm and was subjected to an 18 h hydrothermal reaction at 220°C . The MoS_2 nanoflowers made by the hydrothermal process were composed of uniform crystallinity and size with minimum agglomeration. Zhou et al. [68] have replaced the sulfur source with thioacetamide in their studies. Xia et al., in their recent study, synthesized the $\text{CdS}@\text{MoS}_2$ nanocomposite using the hydrothermal method, and evaluated the photocatalytic degradation of Rhodamine 6G (Rh 6G), and found that adsorption in the nanocomposite increases when the MoS_2 amount is increased, showing a great efficacy in processing Rh 6G [69]. Jian et al. used a two-step hydrothermal method to prepare the nanocomposite $\text{MoS}_2/\text{BiOBr}$, which is very efficient in Rhodamine B (RhB) dye degradation [70].

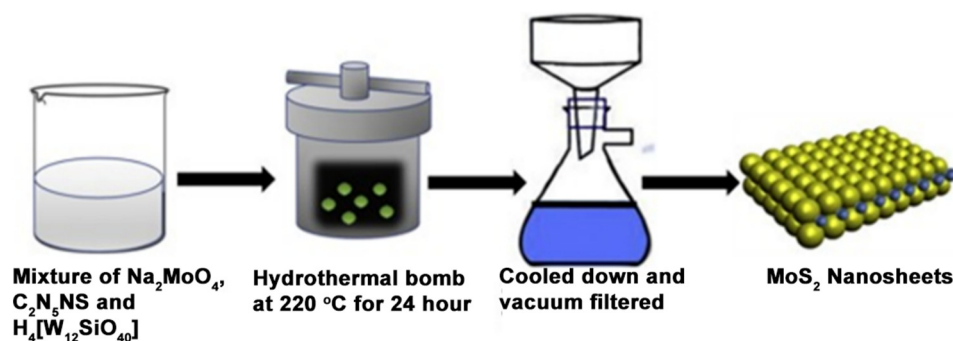


Figure 8. Schematic representation of synthesis of MoS_2 using hydrothermal method [60]. Reprinted with permission from ref. [60]. Copyright 2018-Elsevier.

Additionally, the regulating parameters under hydrothermal parameters are: (a) the percentage of components, (b) the reaction temperature, (c) the solution, (d) the pH value, and (e) the solution concentration. These variables might be effectively controlled to monitor the chemical reaction and the shape of the substance prepared. MoS_2 shows enhanced photothermal properties when synthesized using other processes such as hydrothermal process, a photo-deposition technique, and an in situ solid-state chemical reduction approach. Moreover, at low temperatures, the $\text{Ag}/\text{MoS}_2/\text{TiO}_2\text{-x}$ composite had outstanding degradation properties. Its hydrogen production rate was considerably higher than that of pristine TiO_2 [71].

Solvothermal method: The solvothermal and hydrothermal methods of syntheses are similar techniques [72]. An organic solvent is used in the latter technique instead of water. Thus, where hydrothermal method cannot be applied for compounds that are very easily hydrolyzed, the solvothermal method can be used. In the solvothermal process, non-aqueous solvents are utilized as pressure carriers, intermediates, and mineralizers. Simultaneously, several non-aqueous solvents with a variety of characteristics can be utilized, resulting in nanomaterials with a diverse set of properties. Solvothermal processes

can be used to make core-shell composites. Bai and collaborators generated a $\text{Co}_9\text{S}_8@\text{MoS}_2$ core-shell heterojunction via a solvothermal method, which enhanced the catalytically active sites [73]. Zhang et al. used a basic solvent thermal approach to make MoS_2 /carbon nanotubes with a core-shell structure having improved optical properties [74]. To build $\text{Fe}_3\text{O}_4@\text{SiO}_2@\text{MoS}_2/\text{g-C}_3\text{N}_4$ (FSMG), Lu et al. employed a unique and efficient method where the Fe_3O_4 spheres formed the inner core of the SiO_2 shell—placed using the sol-gel process—and were made using the solvothermal method. FSMG demonstrated good degradation behaviour against RhB when exposed to visible light. Importantly, by adjusting the proportion of water in the solvent, the size of the gel can be easily managed. Gao et al. have reported a solvothermal preparation by mixing MoS_2 from ammonium tetrathiomolybdate with dimethylformamide (DMF) and hydrazine [75]. The mixture was then autoclaved for 10 h with 200°C . The preparation of MoS_2 aggregate is given in Figure 9.

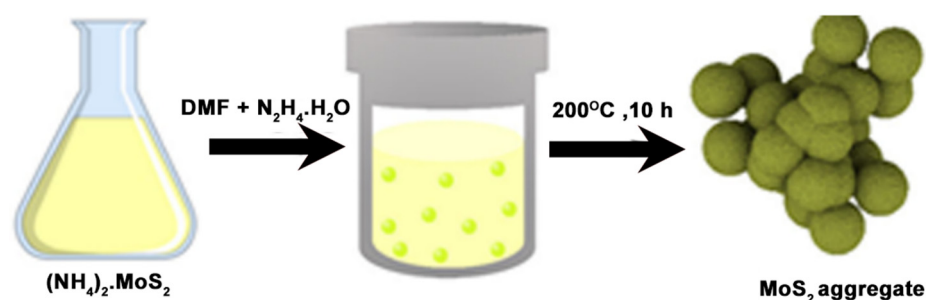


Figure 9. Schematic diagram of solvothermal synthesis of MoS_2 nanosheet aggregates [75]. Reprinted with permission from ref. [75]. Copyright 2018-Nature research.

Other methods: The methods discussed below are some of the most novel ones, namely, (a) thermal-based sulfurization process, (b) ultrasonic-assisted homogenous magnetic stirring method, (c) ultrasound-assisted cracking system, (d) thermal evaporation technique-based systems, (e) in situ growth method, (f) hydrolysis method, and (g) dual-template approach. Hollow structures may be developed using the dual-template approach, where the method increases the active sites and characteristics of produced MoS_2 nanosheets [76]. Thermal sulfurization has been used to create homogeneous MoS_2 films [77]. This approach does not require any pre-processing, unlike chemical vapour deposition (CVD). Acid treatment and ultrasonic irradiation are required before the ultrasound-assisted cracking procedure in order to obtain ideal materials [78]. Hydrolysis is a process for preparing nanoparticles in which precursor molecules are appropriately hydrolyzed in an aqueous solution environment under specific conditions. Zhu et al. reported the synthesis of MoS_2 nanosheets of uniform thickness using a quick and fast LiBH_4 hydrolysis reaction [79].

4. Characterization of MoS_2 -Based Materials

4.1. Morphological Properties

The shape of MoS_2 -based photocatalysts affects their efficiency. Depending on the technique of preparation, MoS_2 can have a variety of morphologies. Jaleel et al. created MoS_2 with a nanoflower shape utilizing a hydrothermal procedure using ammonium molybdate as the Mo source and thiourea as the S source [59]. This nanocomposite was used for degrading the malachite green dye with great efficiency. The SEM image of the nanoflower MoS_2 is given in Figure 10a [59]. Sun et al. used the CVD process to create nanosheets of MoS_2 and the hydrothermal intercalation method to construct nanospheres and used them for the adsorption studies. Figure 10b represents the nanosphere structure of MoS_2 [80]. Visic et al. and co-workers prepared MoS_2 coaxial nanotubes by the sulfurization transition of $\text{M}_6\text{S}_2\text{I}_8$ nanowires in an argon environment with a gas flow of $\text{H}_2/\text{H}_2\text{S}$ mixture. They proposed this MoS_2 as an analogous material to graphene. Figure 10c represents the nano-wired MoS_2 [81]. Mahyavanshi et al. used a chemical vapour deposition technique to

illustrate the directional growth of MoS₂ monolayer ribbons (Figure 10e) in a sulfur-rich environment. An array of molybdenum and sulphur edge terminations with 60° and 120° angle formations are present in this nanocomposite, as evidenced from the SEM and TEM images. There may be new opportunities for electrical and electrochemical applications due to the directed development of MoS₂ ribbons with specified edge structures under specific CVD conditions [82]. The MoS₂ nanoflakes were synthesized by Wu et al., (Figure 10f) via effective grinding-assisted sonication exfoliation for photoluminescence studies of MoS₂ [83]. SEM images of nanoflower, nanosheet, nanosphere, nanotube, nanoribbon, and nanoflake morphologies are depicted in Figure 10a–f, respectively [83]. The HRTEM images in Figure 11a,b shows a close interface between the three components, which could assist with electron transfer to the composite surface [84,85].

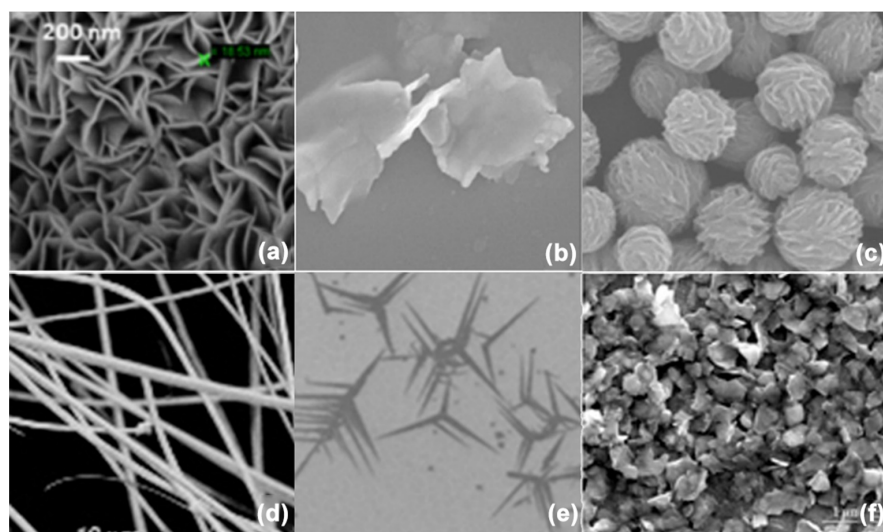


Figure 10. (a) Nanoflower [59], (b) Nanosheets [80], (c) Nanosphere [80], (d) Nanotube [81], (e) Nanoribbon [82], (f) Nanoflakes [83]. Reprinted with permission from ref. [59,80–83]. Copyright 2021-Springer, Copyright 2015-OSA publication, Copyright 2011-Springer, Copyright 2017-Elsevier, Copyright 2014-Hindawi publication.

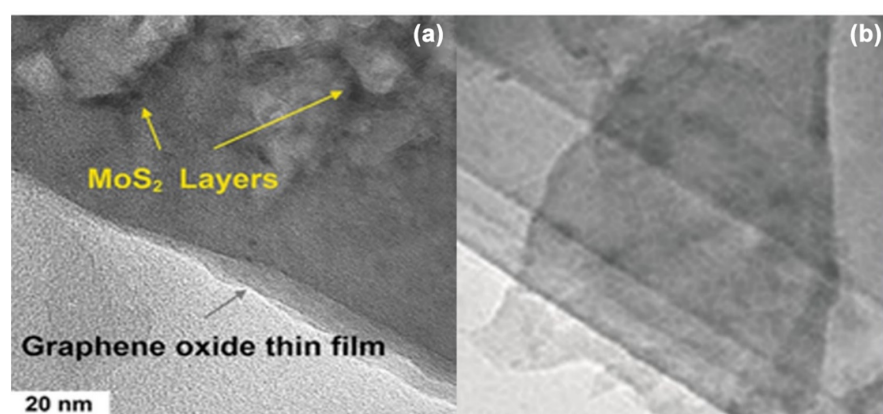


Figure 11. (a,b) TEM images of MoS₂-based system. Reprinted with permission from ref. [84,85] 2015-Nature research, Copyright 2013-Springer.

4.2. Structural Properties

The various characterization techniques used to determine the structure of MoS₂ are discussed here [59,81,86–88].

X-ray diffraction (XRD) has a significant role in identifying the crystalline nature of the material in nanocomposite studies. MoS₂ shows different peaks in the XRD as shown in

Figure 12a. The major plane obtained is (002) at 14.38° [89]. This corresponds to about eight layers of MoS_2 . Besides this major peak, MoS_2 also displays peaks that correspond to (100), (101) at 32° , (103) at 40° , (105) at 49° , (110) at 58.5° , (008), and (200) planes [81]. There is no peak corresponding to (001) plane as there is no MoO_3 [90]. Infrared spectral analysis (FTIR) is the other major characterization tool used to identify the functional groups present in the nanomaterial. As shown in Figure 12b, the FTIR plot of MoS_2 shows various peaks. The peak at 3182 cm^{-1} is due to the O–H group, while 639 cm^{-1} , 893.39 cm^{-1} , 1402.99 cm^{-1} , and 1622.8 cm^{-1} , are the broad absorption bands attributed to MoS_2 . And the band at 483.23 cm^{-1} and 931.39 cm^{-1} are due to S–S bond [88].

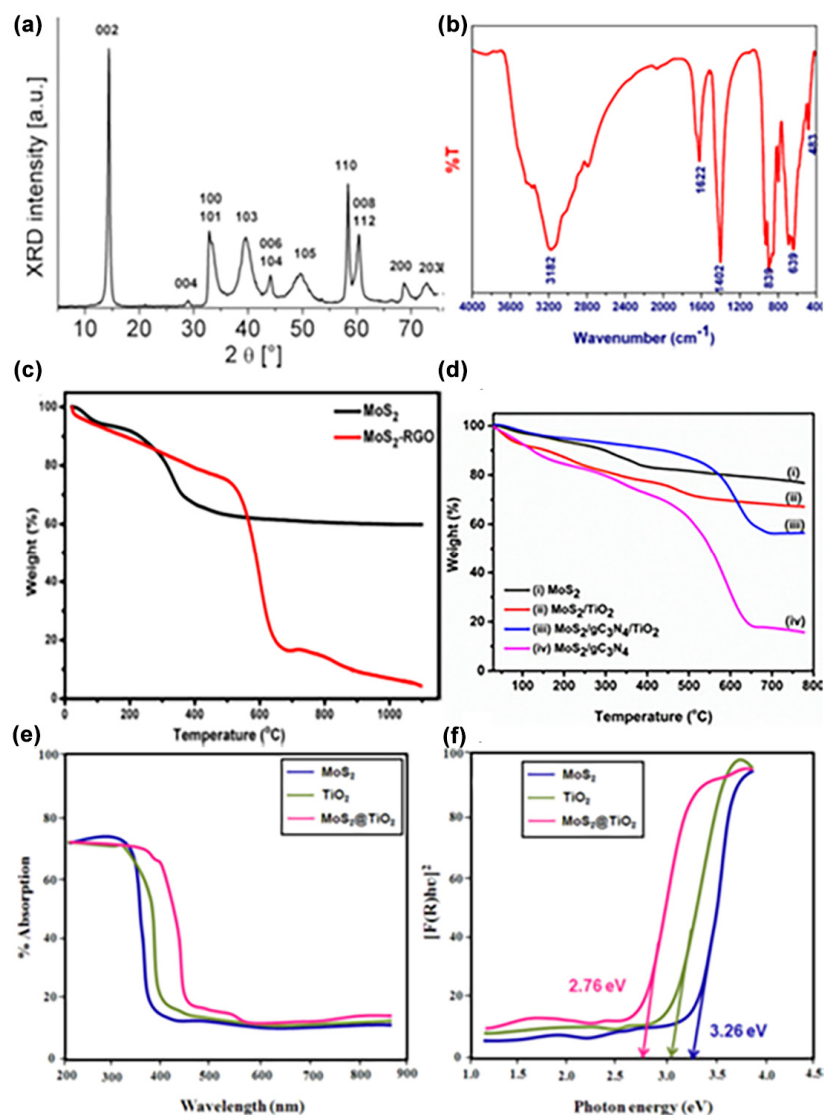


Figure 12. (a) XRD plot of MoS_2 , (b) FTIR plot of MoS_2 , (c,d) TGA curves of MoS_2 , (e) UV-DRS graph of MoS_2 , (f) Tauc plot of MoS_2 . Reprinted with permission from ref. [59,81,86–88]. Copyright 2011-Springer, Copyright 2019-Springer. Copyright 2020-Springer, Copyright 2017-American Chemical Society. Copyright 2020-Springer.

Thermogravimetric analysis (TGA) on the MoS_2 shows the thermal stability of the material. The TGA plot of MoS_2 is given in Figure 12. In Figure 12c,d, we can see a similar pattern of thermal decomposition of the MoS_2 . Bahuguna et al. [87] synthesized MoS_2 using a hydrothermal process and then carried out TGA analysis. MoS_2 shows an initial loss of mass at about 100°C , which is caused by the evaporation of adsorbed water molecules, as seen in Figure 12c. Further, MoS_2 loses mass at around 300°C , due to the decomposition of

sulfur from the compound, and the MoS₂ oxidizes to MoO₃, after which it remains stable up to 1000 °C. Figure 12d(i) shows the TGA analysis of the MoS₂ and its modified system [59].

4.3. Optical Properties

The optical properties are usually characterized by two different characterizing tools (a) photoluminescence (PL) and (b) UV-diffuse reflectance spectroscopy (UV-DRS) study. From the UV-DRS analysis, and Tauc plot, the band gap is calculated using Kubelka–Munk function, which is given in Figure 12e,f. The PL spectrum has an important role in proposing a mechanism in organic dye degradation using nanocomposites. The band gap of MoS₂ using Tauc plot has been calculated for MoS₂ as 3.26 eV [86]. Zhang et al. prepared a ternary system of MoS₂/g-C₃N₄/TiO₂ and calculated the band gap as 2.76 eV. Chakrabarty et al. determined the band gap of RGO-MoS₂ supported NiCo₂O₄ as 2.36 eV [91]. Nayak et al. prepared MoS₂/NiFe layered double hydroxide (LDH), and using Tauc calculation, found 1.86 eV as the band gap [92]. In the modified MoS₂ system, the UV-DRS of the composites displayed a red shift towards the visible light spectrum [93].

5. MoS₂-Based System for Degradation of Organic Dyes

Because of its strong optical absorption, MoS₂ has a wide range of applications in photochemistry, photocatalysis, and photoelectronic research. In electronics, the MoS₂-based materials are used as photodetectors [94], field-effect transistors [95], solar cells [96], chemical sensors [97], and so on. MoS₂ is also used in the transportation of drugs in cancer chemotherapy. Major applications of MoS₂ and MoS₂-based systems in various photocatalytic degradation reactions are discussed here.

5.1. Binary Systems of MoS₂

Graphitic carbon nitride (g-C₃N₄) has been thoroughly explored for its small band gap (2.7 eV), nonmetal characteristics, nontoxicity, ease of availability, and excellent thermal and chemical stability since its debut in 2009 for photocatalytic hydrogen evolution. Many studies have been done by fabricating MoS₂ on g-C₃N₄. Zhang et al. [98] prepared a nanocomposite by fabricating MoS₂ and g-C₃N₄. Here, MoS₂ was prepared by the hydrothermal method. The photocatalytic efficiency of the samples was assessed by measuring their ability to degrade the organic RhB and methyl orange (MO) dyes in aqueous solutions when exposed to visible light. The prepared catalysts showed a satisfactory amount of degradation of these dyes. Benavente et al. [99] synthesized a catalyst ZnO/MoS₂ by a sol-gel method and investigated the degradation of 10 ppm of Methylene blue (MB) dye using visible light for 300 min, resulting in a 75% degradation.

Wang and their colleagues have prepared a binary system of MoS₂ with TiO₂. The MoS₂ is synthesized using a simple hydrothermal method, and their ability to degrade RhB, MB, and MO dyes for 60 min showed activities of 99.6, 96.4, and 87.4%, respectively [100]. Selvaraj et al. [101] have prepared a type-II MoS₂/ZnO composite via the hydrothermal method. It degraded the MB dye using UV light and demonstrated 99% degradation activity. In a recent study by Bargozideh et al. [102], MoS₂ nanoflowers were made using a hydrothermal process and fabricated with BiFeO₃, which showed degradation of 89% on RhB dye.

Ding and co-workers have modified MoS₂ with graphene oxide (GO), and studied for the degradation of MB dye [103]. A total of 10 mg of the nanocomposite was used to study the degradation of MB dye in the presence of visible light. The composite showed a degradation of 99%, which is an enhancement of 20% activity over the pristine MoS₂. In this study, they have synthesized MoS₂ using solvothermal method using n-butyl lithium as solvent. The preparation of GO was carried out by the sol-gel method. Tang et al. [104] in a recent study, prepared modified MoS₂ using SrZrO₃ via the hydrothermal method and studied the photodegradation of the MB dye using visible light irradiation. The degradation efficacy was found to be 99.7% for 15 mg nanocomposite in 25 ppm of MB dye. MoS₂/ZnS synthesized via hydrothermal method have been used for the degradation of MB dye. In total, 10 ppm dye solution along with 50 mg of nanocomposite gave

99.89% degradation activity [105]. In a recent study, Jian et al. constructed a BiOBr loaded MoS₂ and studied the photocatalytic activity on the RhB dye [70]. Using 20 mg of nanocomposite in 10 ppm solution of RhB dye in Xenon arc light achieved 96% efficiency. Liu et al., synthesized a flower-like CeO₂/MoS₂ composite and studied its catalytic activity under visible light for the degradation of MO dye. The nanocomposite showed a 96.1% efficiency in 90 min [106]. Sharma et al., used a biosynthetic approach to construct a 3D/2D CeO₂/MoS₂ nanocomposite [107]. Here, 20 mg of the composite decomposed 20ppm of Methyl violet (MV) dye solution under a visible light source (300 W). The efficiency was found to be 96.25% in 90 min. Wang et al. [108], synthesised a CeO₂/MoS₂ 2D nanostructure via hydrothermal method for the reduction study of aqueous Cr(VI). Then, 6 mg of catalyst and 5ppm of Cr(VI) resulted in a 99% removal of Cr(VI) in 120 min.

From all these studies, it can be seen that the fabrication of effective photocatalysts on MoS₂ reduces the band gap of the final composite prepared. All of the photocatalysts discussed below are semiconductor photocatalysts, where the narrowing of the band gap considerably boosts catalytic activity.

5.2. Ternary Systems of MoS₂

Different oxides have been doped with MoS₂ to increase their degradation efficacy in photocatalysis. g-C₃N₄ is a metal-free semiconductor having a layered structure with great electron-proton transferability and has found applications as a photocatalyst [109]. Incorporating TiO₂ into the binary system above to obtain MoS₂/g-C₃N₄/TiO₂ ternary system has led to a significant increase in the action of MoS₂ and g-C₃N₄ photocatalysts.

Jo et al. synthesized a ternary MoS₂/g-C₃N₄/TiO₂ system in 2015 [110]. The composite was prepared over multiple steps. Initially, MoS₂ was prepared using hydrothermal method and then exfoliated with g-C₃N₄. TiO₂ was added by the impregnation method to obtain MoS₂/g-C₃N₄/TiO₂. In the photocatalytic experiment, to 10 ppm MB, 30 mg of prepared catalyst was added, and the reaction observed for 60 min under visible light irradiation. The system g-C₃N₄ (10%)/TiO₂/MoS₂ (0.2%) showed an activity of 99.5%. Atrazine herbicide degradation has also been studied under the same conditions for 300 min to obtain 86% degradation [110]. In 2016, Zhang et al. [111] fabricated TiO₂/g-C₃N₄/MoS₂ composite from g-C₃N₄ and exfoliated it with hydrothermally synthesized MoS₂ to obtain TiO₂/g-C₃N₄/MoS₂ using solvothermal method and used for MO degradation (20 ppm of MO solution). The degradation of pure TiO₂, pure g-C₃N₄, g-C₃N₄/MoS₂, and TiO₂/g-C₃N₄ was 28.9, 22.4, 26.7, and 90.1%, respectively (100 mg catalyst). In comparison, all TiO₂/g-C₃N₄/MoS₂ composites had better photocatalytic activity than pure TiO₂, g-C₃N₄, and TiO₂/g-C₃N₄ composites, demonstrating that TiO₂ and g-C₃N₄/MoS₂ hybrid had a synergistic impact. The Gaussian09 programme was used to perform DFT investigations on the as-prepared composite photocatalyst for both geometry optimization and frequency estimation [111]. Figure 13 shows the optimized TiO₂/g-C₃N₄/MoS₂ composite structure utilizing the LANL2DZ basis package at the density functional B3LYP level. Following the calculations of the TiO₂, MoS₂, g-C₃N₄, and TiO₂/MoS₂ moieties, the structures of potential TiO₂/g-C₃N₄/MoS₂ combinations were computed using the B3LYP density functional theory with the LANL2D basis set. The B3LYP-D3 method was used to optimize the adsorption energy of a TiO₂/g-C₃N₄/MoS₂ composite.

In 2020, Mahalakshmi et al. reported the g-C₃N₄/MoS₂/TiO₂ system for photodegradation [112]. The g-C₃N₄, synthesized from melamine was added to titanium isopropoxide (TTIP) with rapid stirring. Then the hydrothermally prepared MoS₂ and the above-prepared solutions were added, and hydrothermal synthesis was carried out to obtain a C₃N₄/MoS₂/TiO₂ system. They investigated the catalyst's activity at various weight percentages as well as the degradation of the MO dye. In 0.355 g of MO dye, 50 mg of catalyst was added. Under visible light irradiation, the reaction was carried out for 60 min. The catalyst showed an 88% degradation. The same hybrid catalyst has been used for the degradation of 4-nitrophenol (4-NP) to obtain a degradation efficiency of 74%. In a recent study, Jaleel et al. prepared the nanocomposite MoS₂/g-C₃N₄/TiO₂ using hydrothermal

and exfoliation methods [59]. Here, 50 mg of prepared nanocomposite was added to 50 ppm of malachite green (MG) dye to obtain 97% efficiency within 60 min. The Box–Behnken design of the response surface approach is also used to examine the optimal experimental conditions for dye degradation [59].

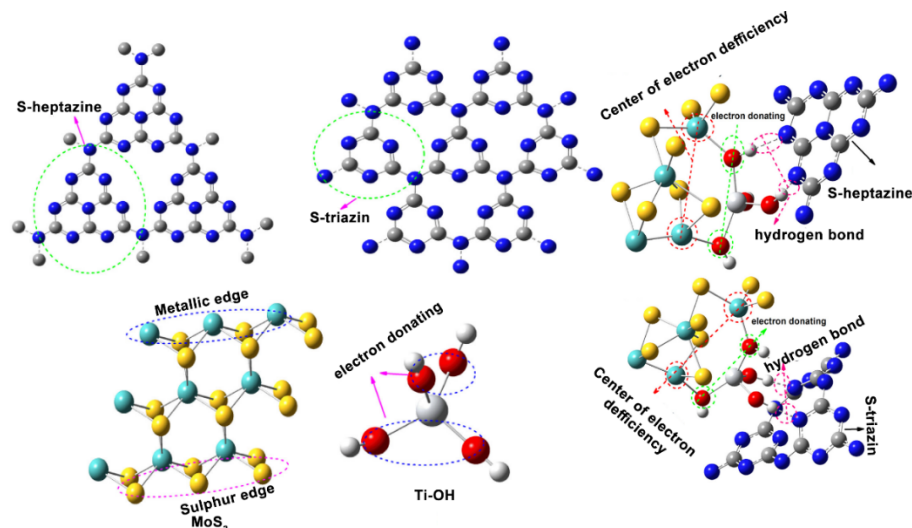


Figure 13. The optimized structure of $\text{TiO}_2/\text{g-C}_3\text{N}_4/\text{MoS}_2$ nanocomposite. (Blue-N, Red-O, White-Ti, Grey-C, Yellow-Mo, Cyan-S) Reprinted with permission from ref. [111]. Copyright 2018-Elsevier.

Modification of MoS_2 nanoparticles with the $\text{g-C}_3\text{N}_4$ and ZnO is also reported. Since the two photocatalysts are well-matched with overlapping band alignments, coupling ZnO with $\text{g-C}_3\text{N}_4$ could yield an excellent heterostructure where increased charge separation takes place [113]. Theoretically, electrons excited from the valence band (VB) to the conduction band (CB) of the $\text{g-C}_3\text{N}_4$ will then migrate to the CB of ZnO , such heterostructures have been shown to have enhanced photocatalytic activity. The $\text{MoS}_2/\text{g-C}_3\text{N}_4/\text{ZnO}$ nanocomposite is used to degrade the MB dye for 60 min, and the MB dye shows more than 90% degradation. Lu et al. [114] synthesized $\text{g-C}_3\text{N}_4$ and Ag on MoS_2 and investigated the degradation activity on the RhB dye for 90 min using a Xenon arc lamp as a light source. The amount of MoS_2 used in this analysis was 100 g, and the dye concentration was 20 ppm to yield a degradation of 95.8%. The MoS_2 has a flower-like morphology and was synthesized using a hydrothermal process.

Beyhaqi and colleagues prepared a nanocomposite by modifying the MoS_2 using $\text{g-C}_3\text{N}_4$ and WO_3 . The photodegradation study was performed on three dyes RhB, MO, and MB using Xenon lamps as the light source. The degradation efficiency obtained was 99.9, 83.4, and 91.8%, respectively, for RhB, MO, and MB. The same nanocomposite could degrade ciprofloxacin drug completely within 2 h of irradiation of Xenon arc as light source [115]. Pant et al. [116] modified MoS_2 using CdS and TiO_2 , and it was used to examine the breakdown of MB dye on carbon nanotubes. The dye degraded completely within 15 min of irradiation with visible light. Vignesh et al. modified MoS_2 using $\text{g-C}_3\text{N}_4$ and Bi_2O_3 and studied the reaction of MB degradation. When the visible light was irradiated for 90 min on the dye (20 ppm) using 50 mg catalyst, it gave a good degradation activity of 98.5% [117]. This nanocomposite was also used for the destruction of *E. coli* and *S. aureus* bacteria. Reusability plays an important role in catalysis. Most of the reports related to MoS_2 -based systems have shown good reusability up to five cycles [59,116,118–120]. Talukar et al., synthesized a ternary hybrid nanoflower $\text{CeO}_2\text{-ZrO}_2@\text{MoS}_2$ to study the sonophotocatalytic degradation of naproxen (NPX) using a visible light source (250 W) LED lamp. In total, 50 ppm of NPX solution yielded an enhanced degradation of 96% in 40 min.

A summary of the MoS_2 nanocomposites and the degradation of various dyes has been given in Table 1 [121–141]. In all these studies, we see that the fabricating/doping agent

changes the degradational activity of the nanocomposite. The band gap shows a red shift in the modified MoS₂, which helps in the better utilization of visible light. The morphology and degradation activities have a direct relationship which in turn depends on the preparation technique. Many authors have done computational and statistical studies to understand the highest degradation efficacy and optimal conditions for the degradation of organic dyes.

Table 1. Comparison of the photocatalytic degradation of various dye using MoS₂-based catalysts.

System	Dye	Reaction Conditions			Degradation (%)	Ref.
		Time (Min)	Light Source	Catalyst Amount (mg)		
MoS ₂ /SnO ₂	MB	90	Visible	20		95.0 [30]
MoS ₂ nanosheets	MB	120	Fluorescent lamp	10	100	49.3 [121]
CeO ₂ -ZrO ₂ @MoS ₂	NPX	40	Visible light		50	96.0 [142]
CeO ₂ /MoS ₂	MO	90	Visible light	25	20	96.1 [106]
3D/2D CeO ₂ /MoS ₂	MV	30	Visible light	20	20	96.25 [107]
Cerium-doped MoS ₂	Cr(IV)	30	Visible light	6	20	40 [108]
MoS ₂ /BiOBr	RhB	30	Xenon arc	20	10	96.0 [70]
MoS ₂ -x nanosheet arrays	RhB	60	Visible		5	97.2 [122]
10% g-C ₃ N ₄ /TiO ₂ /MoS ₂ (0.2)	MB	60	Visible	30	10	99.5 [110]
Layered MoS ₂	MB	90	Visible	50	10	71.0 [133]
TiO ₂ /SnS ₂ /MoS ₂	MB	90	Visible		5	81.8 [135]
TiO ₂ /g-C ₃ N ₄ /MoS ₂	MO	60	Visible	100	20	90.6 [111]
g-C ₃ N ₄ /MoS ₂ /TiO ₂	MO	60	Visible	50	0.03	88.0 [112]
MoS ₂ /g-C ₃ N ₄ /TiO ₂	MG	60	Visible	50	10	86.0 [59]
	RhB					99.6
TiO ₂ /MoS ₂	MB	60	Visible	50	10	96.4 [100]
	MO					87.5
RGO-MoS ₂ supported	RhB	90	Visible	50	10	95.0 [91]
NiCo ₂ O ₄						
SrZrO ₃ /Flower-like MoS ₂	RhB	80	solar	15	25	99.7 [104]
g-C ₃ N ₄ /Ag/MoS ₂	RhB	90	Xenon arc	100	20	95.8 [114]
MoS ₂ /NiFe LDH	RhB	120	Solar	20	20	90.0 [92]
MoS ₂ /COF	RhB	30	Solar	10	20	98.0 [136]
MoS ₂ -GO	MB	60	solar	10	10	99.0 [103]
BiPO ₄ , MoS ₂ and graphene	RhB	90	Mercury	100	5	- [137]
	RhB					99.9
g-C ₃ N ₄ /WO ₃ /MoS ₂	MO		Xenon arc	100	20	83.4 [115]
	MB					20
	MB					91.8
MoS ₂ /CdS/TiO ₂	MB	15	Visible	25	10	100 [116]
g-C ₃ N ₄ -based MoS ₂ and Bi ₂ O ₃	MB	90	Visible	50	20	98.5 [117]
MoS ₂ /ZnS	MB	32	Visible	50	10	99.9 [105]
MoS ₂ /CdIn ₂ S ₄	RhB	30	Visible		10	- [138]
						94.9
CoFe ₂ O ₄ /MoS ₂	CRMBMO	60	Visible	30	20	67.8 [139]
ZnO/MoS ₂	MB	300	Visible	10	1	75.0 [99]
Type II MoS ₂ /ZnO	MB	120	UV		10	99.0 [101]
BiOIO ₃ /MoS ₂ (BM-x) 2D/2D	RhB	90	500 W Xenon lamp	50	10	98.7 [140]
ZnO-MoS ₂	MR	60	Solar	10	10	89.0 [141]
BiFeO ₃ /MoS ₂	RhB	200	Visible	50	10	89.0 [102]
ZnO nanorods/MoS ₂	RhB		UV	-	4	- [123]
	MB					95.3
Ultrathin layered MoS ₂	RhB	36	Visible	100	5	41.1 [124]
MoS ₂ /TiO ₂	MB	12	UV-Vis	50	5	99.3 [125]
TiO ₂ /MoS ₂	MB	30	Visible	10	10	94.2 [126]
NMS						
incorporated Fe ₂ O ₃ /ZnO	RhB	240	Visible	40		91.0 [127]
Ag ₃ PO ₄ /MoS ₂	MB	15	60 W CFL	0.20 g/L	20	97.6 [128]
MoS ₂ /g-C ₃ N ₄	RhB/MO	60	Visible	5	50	92.0 [98]
PbS/MoS ₂	MB	180	Visible	1%	30	83.0 [129]
MoS ₂ QDs@ZnIn ₂ S ₄ @RGO)	RhB/MB	30	300 W Xenon lamp	100	80	98.8 [130]
						98.5
SnO ₂ -MoS ₂	MR/MB	120	Visible	1	100	58.5 [131]
						94.0
MoS ₂ -SrFe ₁₂ O ₁₉	RhB	120	300 W Xenon lamp		10	96.5 [132]
Au-CoFe ₂ O ₄ /MoS ₂	MO	60	300 W iodine tungsten lamp	70	50	96.0 [134]

6. Mechanism of Dye Degradation Using MoS₂-Based Systems

MoS₂, a semiconductor photocatalyst undergoes electron-hole pair recombination during the degradation reaction. The mechanism of the MoS₂-based photocatalyst is described using electron pairs and holes [143]. Based on the different types of electron transfer, the mechanism is classified as traditional and Z-scheme mechanisms. The traditional mechanism of the binary system MoS₂/Cu₂O is given in Figure 14a [144], and the ternary system

MoS₂/CdS/TiO₂ is given in Figure 14c [116]. The Z-scheme mechanism of the binary system MoS₂/g-C₃N₄ [145], and ternary system MoS₂/g-C₃N₄/TiO₂ [59] are shown in Figure 14b,d, respectively. In the traditional mechanism, valence band electrons (e⁻) absorb enough energy to migrate to the conduction band and form holes (h⁺). Because the conduction band of MoS₂ is close to that of TiO₂, photoelectrons released in TiO₂ are transported to MoS₂ more quickly, enabling carrier separation and minimizing the photogenerated electron and hole recombination [126]. In the Z-scheme mechanism [146], the electrons move to CB from VB, and then they will transfer to the VB of the nearest atom. Thus, a zig zag electron transfer is exhibited by these nanocomposites. Mahalakshmi et al. [112] presented an S-scheme mechanism, using MoS₂/g-C₃N₄/TiO₂ catalyst (Figure 14e). During the irradiation of light, electrons from VB of g-C₃N₄, MoS₂, and TiO₂ are stimulated singly to the CB in this process. In the hole of TiO₂'s VB, the excited electrons recombine. The approach helped in the spatial isolation and extraction of photoexcited carriers with larger redox capabilities, and stored electrons of the MoS₂/TiO₂/g-C₃N₄ surface are helpful in the decomposition of organic dyes.

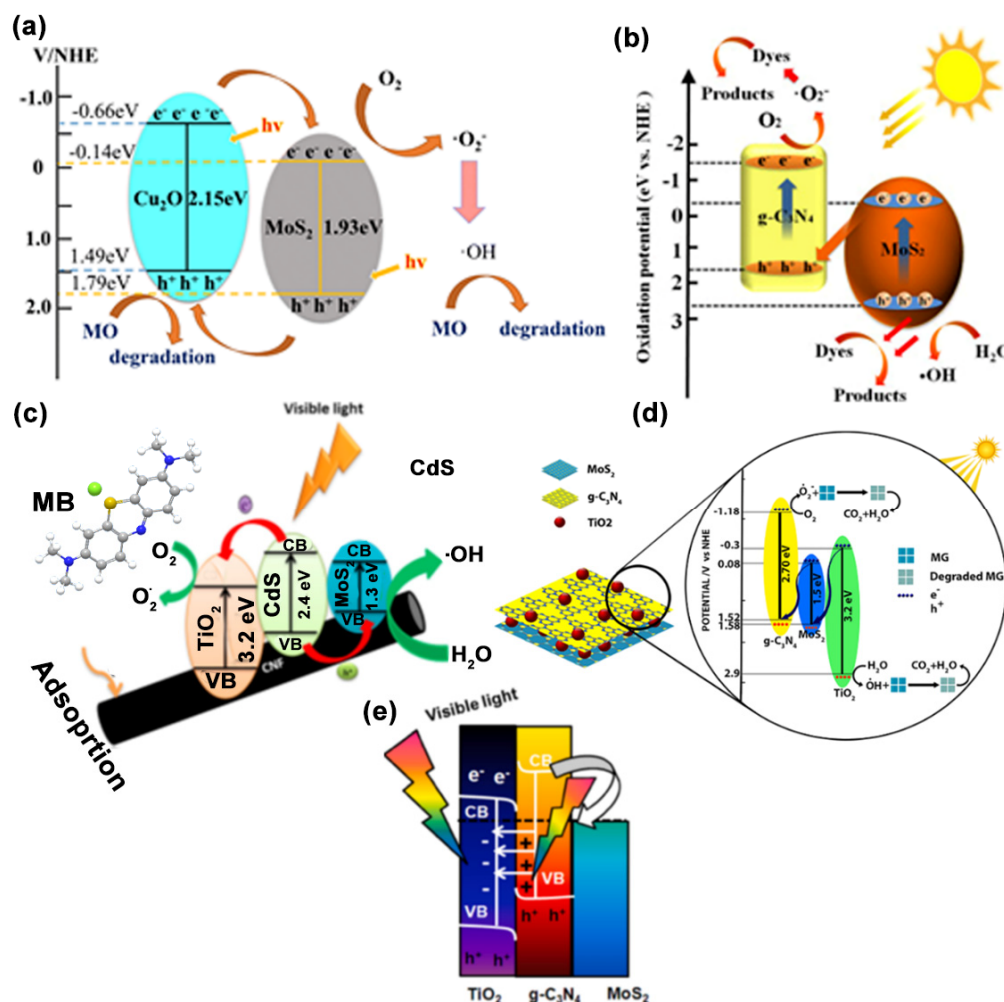


Figure 14. The mechanism of the MoS₂-based photocatalyst on the dye (a) traditional mechanism in binary system MoS₂/Cu₂O [144], (b) Z-scheme mechanism in binary system MoS₂/g-C₃N₄ [145], (c) Traditional mechanism in ternary system MoS₂/CdS/TiO₂ [116], (d) Z-scheme in ternary system MoS₂/g-C₃N₄/TiO₂ [59], and (e) s-scheme in ternary system MoS₂/g-C₃N₄/TiO₂ [112]. Reprinted with permission from ref. [59,112,116,144,145]. Copyright 2021-Springer, Copyright 2020-Elsevier, Copyright 2019-Elsevier, Copyright 2020-Springer, Copyright 2017-Elsevier.

As mentioned earlier, the PL spectra have an important role in identifying the particular mechanism of dye degradation. Figure 15a represents the PL spectrum and its traditional mechanism using $\text{MoS}_2@ \text{TiO}_2$ [86]. Jia et al. have proposed a Z-scheme mechanism based on the PL spectra for the $\text{Au-CoFe}_2\text{O}_4/\text{MoS}_2$ nanocomposite [134]. When the spectral intensity is increased after the fabrication, the nanocomposite chooses a Z-scheme mechanism. At low intensities, the composite chooses a traditional mechanism. The PL spectra and the mechanism are given in Figure 15b. A reduction in PL strength indicates that the electron-hole pair recombination has been suppressed.

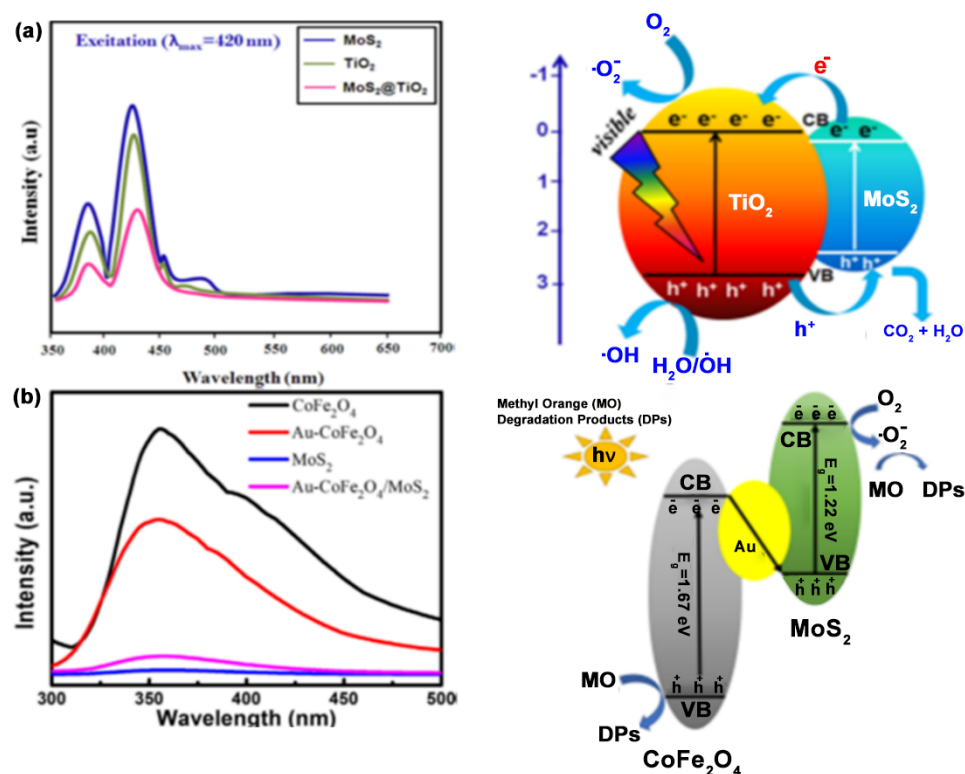


Figure 15. PL spectra and their mechanism (a) Traditional mechanism of $\text{MoS}_2@ \text{TiO}_2$ [86], (b) Z-scheme mechanism of $\text{MoS}_2/\text{CoFe}_2\text{O}_4$ [134]. Reprinted with permission from ref. [86,134]. Copyright 2020-Elsevier, Copyright 2019-Elsevier.

7. Conclusions and Future Perspective

This review has discussed the geometry, polymorphism, different methods of preparation, and characterization, of MoS_2 -based composites for the photocatalytic degradation of organic dyes. MoS_2 -based binary and ternary systems have been considered. The degradation ability depends on factors such as morphology and the preparation techniques employed. The chemical properties of the added components help in the formation of a heterojunction with MoS_2 , leading to an increase in the efficacy of the final catalyst towards the degradation of dyes. Based on the various studies conducted, the photocatalytic activity of MoS_2 -based nanomaterials has the following characteristics. The force of attraction between the various materials used to fabricate the hybrid catalyst, and the crystallographic plane where the fabrication is taking place on the nanomaterial are significant factors affecting their efficiency. The MoS_2 -based nanomaterials show great degradation activity towards organic dyes and toxic pollutants. This area of study offers significant opportunities for fabricating excellent photocatalysts to affect the degradation of organic pollutant dyes from wastewater.

Author Contributions: J.R.J.U.—Methodology, software, investigation, data curation, writing original draft. M.R.—Methodology, investigation, writing original draft. S.D.K.R.—Investigation, writing, review and editing, supervision, project administration. D.P.—Visualization, validation, writing review and editing. M.K.M.—Resource, investigation, data curation, writing, review and editing. All authors have read and agreed to the published version of the manuscript.

Funding: This research received no external funding.

Institutional Review Board Statement: Not applicable.

Informed Consent Statement: Not applicable.

Data Availability Statement: This study did not report any data.

Acknowledgments: The authors are grateful to CHRIST (Deemed to be University) for the esteemed support and encouragement.

Conflicts of Interest: The authors declare no conflict of interest.

References

1. Kroto, H.W.; Heath, J.R.; O'Brien, S.C.; Curl, R.F.; Smalley, R.E. C₆₀: Buckminsterfullerene. *Nature* **1985**, *318*, 162–163. [[CrossRef](#)]
2. Bethune, D.S.; Kiang, C.H.; de Vries, M.S.; Gorman, G.; Savoy, R.; Vazquez, J.; Beyers, R. Cobalt-Catalysed Growth of Carbon Nanotubes with Single-Atomic-Layer Walls. *Nature* **1993**, *363*, 605–607. [[CrossRef](#)]
3. Xie, X.; Kretschmer, K.; Wang, G. Advances in Graphene-Based Semiconductor Photocatalysts for Solar Energy Conversion: Fundamentals and Materials Engineering. *Nanoscale* **2015**, *7*, 13278–13292. [[CrossRef](#)]
4. Wilson, J.A.; Yoffe, A.D. The Transition Metal Dichalcogenides Discussion and Interpretation of the Observed Optical, Electrical and Structural Properties. *Adv. Phys.* **1969**, *18*, 193–335. [[CrossRef](#)]
5. Singh, A.K.; Kumar, P.; Late, D.J.; Kumar, A.; Patel, S.; Singh, J. 2D Layered Transition Metal Dichalcogenides (MoS₂): Synthesis, Applications and Theoretical Aspects. *Appl. Mater. Today* **2018**, *13*, 242–270. [[CrossRef](#)]
6. Zhang, X.; Teng, S.Y.; Loy, A.C.M.; How, B.S.; Leong, W.D.; Tao, X. Transition Metal Dichalcogenides for the Application of Pollution Reduction: A Review. *Nanomaterials* **2020**, *10*, 1012. [[CrossRef](#)]
7. Monga, D.; Sharma, S.; Shetti, N.P.; Basu, S.; Reddy, K.R.; Aminabhavi, T.M. Advances in Transition Metal Dichalcogenide-Based Two-Dimensional Nanomaterials. *Mater. Today Chem.* **2021**, *19*, 100399. [[CrossRef](#)]
8. Agarwal, V.; Chatterjee, K. Recent Advances in the Field of Transition Metal Dichalcogenides for Biomedical Applications. *Nanoscale* **2018**, *10*, 16365–16397. [[CrossRef](#)]
9. Zhang, G.; Liu, H.; Qu, J.; Li, J. Two-Dimensional Layered MoS₂: Rational Design, Properties and Electrochemical Applications. *Energy Environ. Sci.* **2016**, *9*, 1190–1209. [[CrossRef](#)]
10. Gupta, U.; Rao, C.N.R. Hydrogen Generation by Water Splitting Using MoS₂ and Other Transition Metal Dichalcogenides. *Nano Energy* **2017**, *41*, 49–65. [[CrossRef](#)]
11. Yuan, Y.J.; Lu, H.W.; Yu, Z.T.; Zou, Z.G. Noble-Metal-Free Molybdenum Disulfide Cocatalyst for Photocatalytic Hydrogen Production. *ChemSusChem* **2015**, *8*, 4113–4127. [[CrossRef](#)]
12. Jin, X.; Fan, X.; Tian, J.; Cheng, R.; Li, M.; Zhang, L. MoS₂ Quantum Dot Decorated g-C₃N₄ Composite Photocatalyst with Enhanced Hydrogen Evolution Performance. *RSC Adv.* **2016**, *6*, 52611–52619. [[CrossRef](#)]
13. Dhiman, V.; Kondal, N. MoS₂-ZnO Nanocomposites for Photocatalytic Energy Conversion and Solar Applications. *Phys. B* **2022**, *628*, 413569. [[CrossRef](#)]
14. Jiang, Y.; Wu, R.; Zhou, L.; Li, Z.; Tian, L.; Cao, R. Phase Engineering-Defective 1T @ 2H MoS₂ Nanoflowers as Excellent Full Spectrum Photocatalyst. *J. Alloys Compd.* **2022**, *910*, 164898. [[CrossRef](#)]
15. Choi, W.; Choudhary, N.; Han, G.H.; Park, J.; Akinwande, D.; Lee, Y.H. Recent Development of Two-Dimensional Transition Metal Dichalcogenides and Their Applications. *Mater. Today* **2017**, *20*, 116–130. [[CrossRef](#)]
16. Radisavljevic, B.; Radenovic, A.; Brivio, J.; Giacometti, V.; Kis, A. Single-Layer MoS₂ Transistors. *Nat. Nanotechnol.* **2011**, *6*, 147–150. [[CrossRef](#)]
17. Lopez-Sanchez, O.; Lembke, D.; Kayci, M.; Radenovic, A.; Kis, A. Ultrasensitive Photodetectors Based on Monolayer MoS₂. *Nat. Nanotechnol.* **2013**, *8*, 497–501. [[CrossRef](#)]
18. Tongay, S.; Zhou, J.; Ataca, C.; Liu, J.; Kang, J.S.; Matthews, T.S.; You, L.; Li, J.; Grossman, J.C.; Wu, J. Broad-Range Modulation of Light Emission in Two-Dimensional Semiconductors by Molecular Physisorption Gating. *Nano Lett.* **2013**, *13*, 2831–2836. [[CrossRef](#)]
19. Liu, T.; Wang, C.; Gu, X.; Gong, H.; Cheng, L.; Shi, X.; Feng, L.; Sun, B.; Liu, Z. Drug Delivery with PEGylated MoS₂ Nano-Sheets for Combined Photothermal and Chemotherapy of Cancer. *Adv. Mater.* **2014**, *26*, 3433–3440. [[CrossRef](#)]
20. Tian, Y.; Ge, L.; Wang, K.; Chai, Y. Synthesis of Novel MoS₂/g-C₃N₄ Heterojunction Photocatalysts with Enhanced Hydrogen Evolution Activity. *Mater. Charact.* **2014**, *87*, 70–73. [[CrossRef](#)]
21. Lu, Q.; Yu, Y.; Ma, Q.; Chen, B.; Zhang, H. 2D Transition-Metal-Dichalcogenide-Nanosheet-Based Composites for Photocatalytic and Electrocatalytic Hydrogen Evolution Reactions. *Adv. Mater.* **2016**, *28*, 1917–1933. [[CrossRef](#)] [[PubMed](#)]

22. Guardia, L.; Paredes, J.I.; Munuera, J.M.; Villar-Rodil, S.; Ayán-Varela, M.; Martínez-Alonso, A.; Tascón, J.M.D. Chemically Exfoliated MoS₂ Nanosheets as an Efficient Catalyst for Reduction Reactions in the Aqueous Phase. *ACS Appl. Mater. Interfaces* **2014**, *6*, 21702–21710. [[CrossRef](#)] [[PubMed](#)]
23. Hill, E.H.; Zhang, Y.; Whitten, D.G. Aggregation of Cationic P-Phenylene Ethynyls on Laponite Clay in Aqueous Dispersions and Solid Films. *J. Colloid Interface Sci.* **2015**, *449*, 347–356. [[CrossRef](#)]
24. Das, P.; Malho, J.M.; Rahimi, K.; Schacher, F.H.; Wang, B.; Demco, D.E.; Walther, A. Nacre-Mimetics with Synthetic Nanoclays up to Ultrahigh Aspect Ratios. *Nat. Commun.* **2015**, *6*, 5967. [[CrossRef](#)]
25. Dong, J.; Fang, W.; Yuan, H.; Xia, W.; Zeng, X.; Shangguan, W. Few-Layered MoS₂/ZnCdS/ZnS Heterostructures with an Enhanced Photocatalytic Hydrogen Evolution. *ACS Appl. Energy Mater.* **2022**, *5*, 4893–4902. [[CrossRef](#)]
26. Salarizadeh, P.; Askari, M.B.; Di Bartolomeo, A. MoS₂/Ni₃S₂/Reduced Graphene Oxide Nanostructure as an Electrocatalyst for Alcohol Fuel Cells. *ACS Appl. Nano Mater.* **2022**, *5*, 3361–3373. [[CrossRef](#)]
27. Li, Y.; Fu, R.; Duan, Z.; Zhu, C.; Fan, D. Construction of Multifunctional Hydrogel Based on the Tannic Acid-Metal Coating Decorated MoS₂ Dual Nanozyme for Bacteria-Infected Wound Healing. *Bioact. Mater.* **2022**, *9*, 461–474. [[CrossRef](#)]
28. Shen, H.; Liao, S.; Jiang, C.; Zhang, J.; Wei, Q.; Ghiladi, R.A.; Wang, Q. In Situ Grown Bacterial Cellulose/ MoS₂ Composites for Multi-Contaminant Wastewater Treatment and Bacteria Inactivation. *Carbohydr. Polym.* **2022**, *277*, 118853. [[CrossRef](#)]
29. Sivaranjani, P.R.; Janani, B.; Thomas, A.; Raju, L.L.; Khan, S.S. Recent Development in MoS₂-Based Nano-Photocatalyst for the Degradation of Pharmaceutical Active Compounds. *J. Clean. Prod.* **2022**, *352*, 131506. [[CrossRef](#)]
30. Szkoda, M.; Zarach, Z.; Nadolska, M.; Trykowski, G.; Trzciński, K. SnO₂ Nanoparticles Embedded onto MoS₂ Nanoflakes—an Efficient Catalyst for Photodegradation of Methylene Blue and Photoreduction of Hexavalent Chromium. *Electrochim. Acta* **2022**, *414*, 140173. [[CrossRef](#)]
31. Schwarzenbach, R.P.; Egli, T.; Hofstetter, T.B.; Von Gunten, U.; Wehrli, B. Global Water Pollution and Human Health. *Annu. Rev. Environ. Resour.* **2010**, *35*, 109–136. [[CrossRef](#)]
32. Dwivedi, A.K. Researches in Water Pollution: A Review. *Int. Res. J. Nat. Appl. Sci.* **2017**, *4*, 118–142.
33. Pirilä, M.; Saouabe, M.; Ojala, S.; Rathnayake, B.; Drault, F.; Valtanen, A.; Huuhtanen, M.; Brahmi, R.; Keiski, R.L. Photocatalytic Degradation of Organic Pollutants in Wastewater. *Top. Catal.* **2015**, *58*, 1085–1099. [[CrossRef](#)]
34. Wu, F.; Guan, P.; Xu, X.; Kong, Y.; Cao, D.; Yang, J. High Aspect-Ratio of MoS₂ Nanoribbons via a Single-Source Precursor Route for Photocatalytic Degradation. *Mater. Lett.* **2022**, *315*, 131987. [[CrossRef](#)]
35. Liang, Y.; Yu, L. A New Class of Semiconducting Polymers for Bulk Heterojunction Solar Cells with Exceptionally High Performance. *Acc. Chem. Res.* **2010**, *43*, 1227–1236. [[CrossRef](#)] [[PubMed](#)]
36. Kong, D.; Wang, H.; Cha, J.J.; Pasta, M.; Koski, K.J.; Yao, J.; Cui, Y. Synthesis of MoS₂ and MoSe₂ Films with Vertically Aligned Layers. *Nano Lett.* **2013**, *13*, 1341–1347. [[CrossRef](#)]
37. Kumar, D.P.; Kim, E.H.; Park, H.; Chun, S.Y.; Gopannagari, M.; Bhavani, P.; Reddy, D.A.; Song, J.K.; Kim, T.K. Tuning Band Alignments and Charge-Transport Properties through MoSe₂ Bridging between MoS₂ and Cadmium Sulfide for Enhanced Hydrogen Production. *ACS Appl. Mater. Interfaces* **2018**, *10*, 26153–26161. [[CrossRef](#)]
38. Yuan, Y.; Guo, R.; Hong, L.; Ji, X.; Li, Z.; Lin, Z.; Pan, W. Recent Advances and Perspectives of MoS₂-Based Materials for Photocatalytic Dyes Degradation: A Review. *Colloids Surf. A Physicochem. Eng. Asp.* **2021**, *611*, 125836. [[CrossRef](#)]
39. Ding, Q.; Song, B.; Xu, P.; Jin, S. Efficient Electrocatalytic and Photoelectrochemical Hydrogen Generation Using MoS₂ and Related Compounds. *Chem* **2016**, *1*, 699–726. [[CrossRef](#)]
40. Wypych, F.; Weber, T.; Prins, R. Scanning Tunneling Microscopic Investigation of K_x(H₂O)_y MoS₂. *Surf. Sci.* **1997**, *380*, L474–L478. [[CrossRef](#)]
41. El-Mahalawy, S.H.; Evans, B.L. The Thermal Expansion of 2H-MoS₂, 2H-MoSe₂ and 2H-WSe₂ between 20 and 800 °C. *J. Appl. Crystallogr.* **1976**, *9*, 403–406. [[CrossRef](#)]
42. Arif Khalil, R.M.; Hussain, F.; Manzoor Rana, A.; Imran, M.; Murtaza, G. Comparative Study of Polytype 2H-MoS₂ and 3R-MoS₂ Systems by Employing DFT. *Phys. E Low-Dimens. Syst. Nanostruct.* **2019**, *106*, 338–345. [[CrossRef](#)]
43. Lin, L.; Miao, N.; Huang, J.; Zhang, S.; Zhu, Y.; Horsell, D.D.; Ghosez, P.; Sun, Z.; Allwood, D.A. A Photocatalyst of Sulphur Depleted Monolayered Molybdenum Sulfide Nanocrystals for Dye Degradation and Hydrogen Evolution Reaction. *Nano Energy* **2017**, *38*, 544–552. [[CrossRef](#)]
44. Nguyen, T.N.; Kampouri, S.; Valizadeh, B.; Luo, W.; Ongari, D.; Planes, O.M.; Züttel, A.; Smit, B.; Stylianou, K.C. Photocatalytic Hydrogen Generation from a Visible-Light-Responsive Metal-Organic Framework System: Stability versus Activity of Molybdenum Sulfide Cocatalysts. *ACS Appl. Mater. Interfaces* **2018**, *10*, 30035–30039. [[CrossRef](#)]
45. Rao, C.N.R.; Maitra, U.; Waghmare, U.V. Extraordinary Attributes of 2-Dimensional MoS₂ Nanosheets. *Chem. Phys. Lett.* **2014**, *609*, 172–183. [[CrossRef](#)]
46. Jain, A.; Ong, S.P.; Hautier, G.; Chen, W.; Richards, W.D.; Dacek, S.; Cholia, S.; Gunter, D.; Skinner, D.; Ceder, G.; et al. Commentary: The Materials Project: A Materials Genome Approach to Accelerating Materials Innovation. *APL Mater.* **2013**, *1*, 011002. [[CrossRef](#)]
47. Yu, H.; Zhu, H.; Dargusch, M.; Huang, Y. A Reliable and Highly Efficient Exfoliation Method for Water-Dispersible MoS₂ Nanosheet. *J. Colloid Interface Sci.* **2018**, *514*, 642–647. [[CrossRef](#)]
48. Funke, S.; Miller, B.; Parzinger, E.; Thiesen, P.; Holleitner, A.W.; Wurstbauer, U. Imaging Spectroscopic Ellipsometry of MoS₂. *J. Phys. Condens. Matter* **2016**, *28*, 385301. [[CrossRef](#)]

49. Ghasemi, F.; Abdollahi, A.; Mohajerzadeh, S. Controlled Plasma Thinning of Bulk MoS₂ Flakes for Photodetector Fabrication. *ACS Omega* **2019**, *4*, 19693–19704. [[CrossRef](#)]
50. Zheng, J.; Yan, X.; Lu, Z.; Qiu, H.; Xu, G.; Zhou, X.; Wang, P.; Pan, X.; Liu, K.; Jiao, L. High-Mobility Multilayered MoS₂ Flakes with Low Contact Resistance Grown by Chemical Vapor Deposition. *Adv. Mater.* **2017**, *29*, 1604540. [[CrossRef](#)]
51. Zhou, Q.; Su, S.; Hu, D.; Lin, L.; Yan, Z.; Gao, X.; Zhang, Z.; Liu, J.-M. Ultrathin MoS₂-Coated Ag@Si Nanosphere Arrays as an Efficient and Stable Photocathode for Solar-Driven Hydrogen Production. *Nanotechnology* **2018**, *29*, 105402. [[CrossRef](#)] [[PubMed](#)]
52. Agafonov, V.; Nargelienė, V.; Balakauskas, S.; Bukauskas, V.; Kamarauskas, M.; Lukša, A.; Mironas, A.; Rėza, A.; Šetkus, A. Single Variable Defined Technology Control of the Optical Properties in MoS₂ Films with Controlled Number of 2D-Layers. *Nanotechnology* **2020**, *31*, 025602. [[CrossRef](#)] [[PubMed](#)]
53. Amani, M.; Burke, R.A.; Ji, X.; Zhao, P.; Lien, D.H.; Taheri, P.; Ahn, G.H.; Kirya, D.; Ager, J.W.; Yablonovitch, E.; et al. High Luminescence Efficiency in MoS₂ Grown by Chemical Vapor Deposition. *ACS Nano* **2016**, *10*, 6535–6541. [[CrossRef](#)] [[PubMed](#)]
54. Zhang, X.; Nan, H.; Xiao, S.; Wan, X.; Ni, Z.; Gu, X.; Ostrikov, K. Shape-Uniform, High-Quality Monolayered MoS₂ Crystals for Gate-Tunable Photoluminescence. *ACS Appl. Mater. Interfaces* **2017**, *9*, 42121–42130. [[CrossRef](#)] [[PubMed](#)]
55. Alharbi, A.; Armstrong, D.; Alharbi, S.; Shahrjerdi, D. Physically Unclonable Cryptographic Primitives by Chemical Vapor Deposition of Layered MoS₂. *ACS Nano* **2017**, *11*, 12772–12779. [[CrossRef](#)] [[PubMed](#)]
56. Balendhran, S.; Ou, J.Z.; Bhaskaran, M.; Sriram, S.; Ippolito, S.; Vasic, Z.; Kats, E.; Bhargava, S.; Zhuiykov, S.; Kalantar-Zadeh, K. Atomically Thin Layers of MoS₂ via a Two Step Thermal Evaporation-Exfoliation Method. *Nanoscale* **2012**, *4*, 461–466. [[CrossRef](#)]
57. Qi, H.; Wang, L.; Sun, J.; Long, Y.; Hu, P.; Liu, F.; He, X. Production Methods of Van Der Waals Heterostructures Based on Transition Metal Dichalcogenides. *Crystals* **2018**, *8*, 35. [[CrossRef](#)]
58. Wang, J.; Li, T.; Wang, Q.; Wang, W.; Shi, R.; Wang, N.; Amini, A.; Cheng, C. Controlled Growth of Atomically Thin Transition Metal Dichalcogenides via Chemical Vapor Deposition Method. *Mater. Today Adv.* **2020**, *8*, 100098. [[CrossRef](#)]
59. Jaleel, U.C.; Devi, K.R.; Madhushree, P. Statistical and Experimental Studies of MoS₂/g-C₃N₄/TiO₂: A Ternary Z-Scheme Hybrid Composite. *J. Mater. Sci.* **2021**, *56*, 6922–6944. [[CrossRef](#)]
60. Chaudhary, N.; Khanuja, M.; Abid; Islam, S.S. Hydrothermal Synthesis of MoS₂ Nanosheets for Multiple Wavelength Optical Sensing Applications. *Sens. Actuators A Phys.* **2018**, *277*, 190–198. [[CrossRef](#)]
61. Li, G.; Li, C.; Tang, H.; Cao, K.; Chen, J.; Wang, F.; Jin, Y. Synthesis and Characterization of Hollow MoS₂ Microspheres Grown from MoO₃ Precursors. *J. Alloys Compd.* **2010**, *501*, 275–281. [[CrossRef](#)]
62. Wang, D.; Pan, Z.; Wu, Z.; Wang, Z.; Liu, Z. Hydrothermal Synthesis of MoS₂ Nanoflowers as Highly Efficient Hydrogen Evolution Reaction Catalysts. *J. Power Sources* **2014**, *264*, 229–234. [[CrossRef](#)]
63. Song, X.C.; Zheng, Y.F.; Zhao, Y.; Yin, H.Y. Hydrothermal Synthesis and Characterization of CNT@MoS₂ Nanotubes. *Mater. Lett.* **2006**, *60*, 2346–2348. [[CrossRef](#)]
64. Liu, C.; Wang, Q.; Jia, F.; Song, S. Adsorption of Heavy Metals on Molybdenum Disulfide in Water: A Critical Review. *J. Mol. Liq.* **2019**, *292*, 111390. [[CrossRef](#)]
65. Zou, X.; Zhang, J.; Zhao, X.; Zhang, Z. MoS₂/RGO Composites for Photocatalytic Degradation of Ranitidine and Elimination of NDMA Formation Potential under Visible Light. *Chem. Eng. J.* **2020**, *383*, 123084. [[CrossRef](#)]
66. Anwer, S.; Huang, Y.; Li, B.; Govindan, B.; Liao, K.; Cantwell, W.J.; Wu, F.; Chen, R.; Zheng, L. Nature-Inspired, Graphene-Wrapped 3D MoS₂ Ultrathin Microflower Architecture as a High-Performance Anode Material for Sodium-Ion Batteries. *ACS Appl. Mater. Interfaces* **2019**, *11*, 22323–22331. [[CrossRef](#)]
67. Xie, J.; Zhang, J.; Li, S.; Grote, F.; Zhang, X.; Zhang, H.; Wang, R.; Lei, Y.; Pan, B.; Xie, Y. Controllable Disorder Engineering in Oxygen-Incorporated MoS₂ Ultrathin Nanosheets for Efficient Hydrogen Evolution. *J. Am. Chem. Soc.* **2013**, *135*, 17881–17888. [[CrossRef](#)]
68. Zhou, X.; Xu, B.; Lin, Z.; Shu, D.; Ma, L. Hydrothermal Synthesis of Flower-like MoS₂ nanospheres for Electrochemical Supercapacitors. *J. Nanosci. Nanotechnol.* **2014**, *14*, 7250–7254. [[CrossRef](#)]
69. Xia, J.; Ren, X.; Zhao, L.; Tang, M.; Tan, L.; Fu, C.; Wu, Q.; Ren, J.; Ding, M.; Meng, X. Synthesis of MoS₂ Nanoflowers on CdS Nanorods with a Simple Route and Their Application in Removal of Dyes. *J. Nanoparticle Res.* **2022**, *24*, 1–9. [[CrossRef](#)]
70. Jian, R.; Liu, J.; Wu, Z.; Zheng, H.; Zhu, K.; Sun, Z. Constructing Z-Scheme Structure by Loading BiOBr with (010) Exposure on the Surface of MoS₂ and Its Enhanced Photocatalytic Property for Degrading RhB. *J. Mater. Sci. Mater. Electron.* **2022**, *33*, 6722–6733. [[CrossRef](#)]
71. Zhao, T.; Xing, Z.; Xiu, Z.; Li, Z.; Chen, P.; Zhu, Q.; Zhou, W. Synergistic Effect of Surface Plasmon Resonance, Ti³⁺ and Oxygen Vacancy Defects on Ag/ MoS₂/TiO_{2-x} Ternary Heterojunctions with Enhancing Photothermal Catalysis for Low-Temperature Wastewater Degradation. *J. Hazard. Mater.* **2019**, *364*, 117–124. [[CrossRef](#)] [[PubMed](#)]
72. Aliofkhaezai, M. *Handbook of Nanoparticles*; Aliofkhaezai, M., Ed.; Springer International Publishing: Cham, Switzerland, 2016; ISBN 978-3-319-15337-7.
73. Bai, J.; Meng, T.; Guo, D.; Wang, S.; Mao, B.; Cao, M. Co₉S₈@MoS₂ Core-Shell Heterostructures as Trifunctional Electrocatalysts for Overall Water Splitting and Zn-Air Batteries. *ACS Appl. Mater. Interfaces* **2018**, *10*, 1678–1689. [[CrossRef](#)] [[PubMed](#)]
74. Zhang, X.; Selkirk, A.; Zhang, S.; Huang, J.; Li, Y.; Xie, Y.; Dong, N.; Cui, Y.; Zhang, L.; Blau, W.J.; et al. MoS₂/Carbon Nanotube Core-Shell Nanocomposites for Enhanced Nonlinear Optical Performance. *Chem.-A Eur. J.* **2017**, *23*, 3321–3327. [[CrossRef](#)] [[PubMed](#)]

75. Gao, M.R.; Liang, J.X.; Zheng, Y.R.; Xu, Y.F.; Jiang, J.; Gao, Q.; Li, J.; Yu, S.H. An Efficient Molybdenum Disulfide/Cobalt Diselenide Hybrid Catalyst for Electrochemical Hydrogen Generation. *Nat. Commun.* **2015**, *6*, 5982. [[CrossRef](#)]
76. Zheng, S.; Zheng, L.; Zhu, Z.; Chen, J.; Kang, J.; Huang, Z.; Yang, D. MoS₂ Nanosheet Arrays Rooted on Hollow RGO Spheres as Bifunctional Hydrogen Evolution Catalyst and Supercapacitor Electrode. *Nano-Micro Lett.* **2018**, *10*, 62. [[CrossRef](#)]
77. Antonelou, A.; Syrokostas, G.; Sygellou, L.; Leftheriotis, G.; Dracopoulos, V.; Yannopoulos, S.N. Facile, Substrate-Scale Growth of Mono- and Few-Layer Homogeneous MoS₂ Films on Mo Foils with Enhanced Catalytic Activity as Counter Electrodes in DSSCs. *Nanotechnology* **2015**, *27*, 45404. [[CrossRef](#)]
78. Zheng, X.; Zhu, L.; Yan, A.; Bai, C.; Xie, Y. Ultrasound-Assisted Cracking Process to Prepare MoS₂ Nanorods. *Ultrason. Sonochem.* **2004**, *11*, 83–88. [[CrossRef](#)]
79. Zhu, J.; Wang, H.; Liu, J.; Ouyang, L.; Zhu, M. Exfoliation of MoS₂ and H-BN Nanosheets by Hydrolysis of LiBH₄. *Nanotechnology* **2017**, *28*, 115604. [[CrossRef](#)]
80. Sun, Y.; Xu, J.; Zhu, Z.; Wang, Y.; Xia, H.; You, Z.; Lee, C.; Tu, C. Comparison of MoS₂ Nanosheets and Hierarchical Nanospheres in the Application of Pulsed Solid-State Lasers. *Opt. Mater. Express* **2015**, *5*, 2924. [[CrossRef](#)]
81. Vasic, B.; Dominko, R.; Gunde, M.K.; Hauptman, N.; Skapin, S.D.; Remskar, M. Optical Properties of Exfoliated MoS₂ Coaxial Nanotubes-Analogues of Graphene. *Nanoscale Res. Lett.* **2011**, *6*, 593. [[CrossRef](#)]
82. Mahyavanshi, R.D.; Kalita, G.; Sharma, K.P.; Kondo, M.; Dewa, T.; Kawahara, T.; Tanemura, M. Synthesis of MoS₂ Ribbons and Their Branched Structures by Chemical Vapor Deposition in Sulfur-Enriched Environment. *Appl. Surf. Sci.* **2017**, *409*, 396–402. [[CrossRef](#)]
83. Wu, J.-Y.; Lin, M.-N.; Wang, L.-D.; Zhang, T. Photoluminescence of MoS₂ Prepared by Effective Grinding-Assisted Sonication Exfoliation. *J. Nanomater.* **2014**, *2014*, 1–7.
84. Shi, Y.; Li, H.; Wong, J.I.; Zhang, X.; Wang, Y.; Song, H.; Yang, H.Y. MoS₂ Surface Structure Tailoring via Carbonaceous Promoter. *Sci. Rep.* **2015**, *5*, 10378. [[CrossRef](#)]
85. Gao, D.; Si, M.; Li, J.; Zhang, J.; Zhang, Z.; Yang, Z.; Xue, D. Ferromagnetism in Freestanding MoS₂ Nanosheets. *Nanoscale Res. Lett.* **2013**, *8*, 129. [[CrossRef](#)]
86. Mahalakshmi, G.; Rajeswari, M.; Ponnarasi, P. Fabrication of Dandelion Clock-Inspired Preparation of Core-Shell TiO₂ @ MoS₂ Composites for Unprecedented High Visible Light-Driven Photocatalytic Performance. *J. Mater. Sci. Mater. Electron.* **2020**, *31*, 22252–22264. [[CrossRef](#)]
87. Bahuguna, A.; Kumar, S.; Sharma, V.; Reddy, K.L.; Bhattacharyya, K.; Ravikumar, P.C.; Krishnan, V. Nanocomposite of MoS₂-RGO as Facile, Heterogeneous, Recyclable, and Highly Efficient Green Catalyst for One-Pot Synthesis of Indole Alkaloids. *ACS Sustain. Chem. Eng.* **2017**, *5*, 8551–8567. [[CrossRef](#)]
88. Lalithambika, K.C.; Shanmugapriya, K.; Sriram, S. Photocatalytic Activity of MoS₂ Nanoparticles: An Experimental and DFT Analysis. *Appl. Phys. A Mater. Sci. Process.* **2019**, *125*, 817. [[CrossRef](#)]
89. Rasamani, K.D.; Alimohammadi, F.; Sun, Y. Interlayer-Expanded MoS₂. *Mater. Today* **2017**, *20*, 83–91. [[CrossRef](#)]
90. Balakumar, S.; Rakkesh, R.A.; Prasad, A.K.; Dash, S.; Tyagi, A.K. Nanoplatelet Structures of MoO₃ for H₂ Gas Sensors. In Proceedings of the International Conference on Nanoscience, Engineering and Technology (ICONSET 2011), Chennai, India, 28–30 November 2011; IEEE: Chennai, India, 2011; pp. 514–517.
91. Chakrabarty, S.; Mukherjee, A.; Basu, S. RGO- MoS₂ Supported NiCo₂O₄ Catalyst toward Solar Water Splitting and Dye Degradation. *ACS Sustain. Chem. Eng.* **2018**, *6*, 5238–5247. [[CrossRef](#)]
92. Nayak, S.; Swain, G.; Parida, K. Enhanced Photocatalytic Activities of RhB Degradation and H₂ Evolution from in Situ Formation of the Electrostatic Heterostructure MoS₂/NiFe LDH Nanocomposite through the Z-Scheme Mechanism via p–n Heterojunctions. *ACS Appl. Mater. Interfaces* **2019**, *11*, 20923–20942. [[CrossRef](#)]
93. Rubio, E.J.; Ramana, C.V. Tungsten-Incorporation Induced Red-Shift in the Bandgap of Gallium Oxide Thin Films. *Appl. Phys. Lett.* **2013**, *102*, 191913. [[CrossRef](#)]
94. Zhang, W.; Chuu, C.P.; Huang, J.K.; Chen, C.H.; Tsai, M.L.; Chang, Y.H.; Liang, C.T.; Chen, Y.Z.; Chueh, Y.L.; He, J.H.; et al. Ultrahigh-Gain Photodetectors Based on Atomically Thin Graphene- MoS₂ Heterostructures. *Sci. Rep.* **2015**, *4*, 3826. [[CrossRef](#)] [[PubMed](#)]
95. Das, S.; Chen, H.Y.; Penumatcha, A.V.; Appenzeller, J. High Performance Multilayer MoS₂ Transistors with Scandium Contacts. *Nano Lett.* **2013**, *13*, 100–105. [[CrossRef](#)] [[PubMed](#)]
96. Tsai, M.L.; Su, S.H.; Chang, J.K.; Tsai, D.S.; Chen, C.H.; Wu, C.I.; Li, L.J.; Chen, L.J.; He, J.H. Monolayer MoS₂ Heterojunction Solar Cells. *ACS Nano* **2014**, *8*, 8317–8322. [[CrossRef](#)]
97. Late, D.J.; Huang, Y.K.; Liu, B.; Acharya, J.; Shirodkar, S.N.; Luo, J.; Yan, A.; Charles, D.; Waghmare, U.V.; Dravid, V.P.; et al. Sensing Behavior of Atomically Thin-Layered MoS₂ Transistors. *ACS Nano* **2013**, *7*, 4879–4891. [[CrossRef](#)]
98. Li, Q.; Zhang, N.; Yang, Y.; Wang, G.; Ng, D.H.L. High Efficiency Photocatalysis for Pollutant Degradation with MoS₂/C₃N₄ Heterostructures. *Langmuir* **2014**, *30*, 8965–8972. [[CrossRef](#)]
99. Benavente, E.; Durán, F.; Sotomayor-Torres, C.; González, G. Heterostructured Layered Hybrid ZnO/MoS₂ Nanosheets with Enhanced Visible Light Photocatalytic Activity. *J. Phys. Chem. Solids* **2018**, *113*, 119–124. [[CrossRef](#)]
100. Wang, C.; Zhan, Y.; Wang, Z. TiO₂, MoS₂, and TiO₂/MoS₂ Heterostructures for Use in Organic Dyes Degradation. *ChemistrySelect* **2018**, *3*, 1713–1718. [[CrossRef](#)]

101. Selvaraj, R.; Kalimuthu, K.R.; Kalimuthu, V. A Type-II MoS₂ /ZnO Heterostructure with Enhanced Photocatalytic Activity. *Mater. Lett.* **2019**, *243*, 183–186. [[CrossRef](#)]
102. Bargozideh, S.; Tasviri, M.; Kianifar, M. Construction of Novel Magnetic BiFeO₃/MoS₂ Composite for Enhanced Visible-Light Photocatalytic Performance towards Purification of Dye Pollutants. *Int. J. Environ. Anal. Chem.* **2020**, *2020*, 1–15. [[CrossRef](#)]
103. Ding, Y.; Zhou, Y.; Nie, W.; Chen, P. MoS₂–GO Nanocomposites Synthesized via a Hydrothermal Hydrogel Method for Solar Light Photocatalytic Degradation of Methylene Blue. *Appl. Surf. Sci.* **2015**, *357*, 1606–1612. [[CrossRef](#)]
104. Tang, J.; Shi, Y.; Cai, W.; Liu, F. Construction of Embedded Heterostructured SrZrO₃ /Flower-like MoS₂ with Enhanced Dye Photodegradation under Solar-Simulated Light Illumination. *ACS Omega* **2020**, *5*, 9576–9584. [[CrossRef](#)] [[PubMed](#)]
105. Harish, S.; Archana, J.; Navaneethan, M.; Shimomura, M.; Ikeda, H. Applied Surface Science Synergistic Interaction of 2D Layered MoS₂ /ZnS Nanocomposite for Highly Efficient Photocatalytic Activity under Visible Light Irradiation. *Appl. Surf. Sci.* **2019**, *488*, 36–45. [[CrossRef](#)]
106. Liu, X.; Meng, F.; Yu, B.; Wu, H. Self-Assembly Synthesis of Flower-like CeO₂/MoS₂ Heterojunction with Enhancement of Visible Light Photocatalytic Activity for Methyl Orange. *J. Mater. Sci. Mater. Electron.* **2020**, *31*, 6690–6697. [[CrossRef](#)]
107. Sharma, Y. Biosynthesis of 3D/2D CeO₂/MoS₂ Nanocomposites with Enhanced Photocatalytic Activity to Degrade Organic Dye in Wastewater and Statistical Optimization of Reaction Parameters. *Res. Sq.* **2021**, *1*, 1–21.
108. Wang, H.; Wen, F.; Li, X.; Gan, X.; Yang, Y.; Chen, P.; Zhang, Y. Cerium-Doped MoS₂ Nanostructures: Efficient Visible Photocatalysis for Cr(VI) Removal. *Sep. Purif. Technol.* **2016**, *170*, 190–198. [[CrossRef](#)]
109. Inagaki, M.; Tsumura, T.; Kinumoto, T.; Toyoda, M. Graphitic Carbon Nitrides (g-C₃N₄) with Comparative Discussion to Carbon Materials. *Carbon N. Y.* **2019**, *141*, 580–607. [[CrossRef](#)]
110. Jo, W.K.; Adinaveen, T.; Vijaya, J.J.; Sagaya Selvam, N.C. Synthesis of MoS₂ Nanosheet Supported Z-Scheme TiO₂/g-C₃N₄ Photocatalysts for the Enhanced Photocatalytic Degradation of Organic Water Pollutants. *RSC Adv.* **2016**, *6*, 10487–10497. [[CrossRef](#)]
111. Zhang, W.; Xiao, X.; Li, Y.; Zeng, X.; Zheng, L.; Wan, C. Liquid-Exfoliation of Layered MoS₂ for Enhancing Photocatalytic Activity of TiO₂/g-C₃N₄ Photocatalyst and DFT Study. *Appl. Surf. Sci.* **2016**, *389*, 496–506. [[CrossRef](#)]
112. Mahalakshmi, G.; Rajeswari, M.; Ponnarasi, P. Synthesis of Few-Layer g-C₃N₄ Nanosheets-Coated MoS₂/TiO₂ Heterojunction Photocatalysts for Photo-Degradation of Methyl Orange (MO) and 4-Nitrophenol (4-NP) Pollutants. *Inorg. Chem. Commun.* **2020**, *120*, 108146. [[CrossRef](#)]
113. Zhang, J.; Zhang, M.; Sun, R.-Q.; Wang, X. A Facile Band Alignment of Polymeric Carbon Nitride Semiconductors to Construct Iso-type Heterojunctions. *Angew. Chemie Int. Ed.* **2012**, *51*, 10145–10149. [[CrossRef](#)] [[PubMed](#)]
114. Lu, D.; Wang, H.; Zhao, X.; Kondamareddy, K.K.; Ding, J.; Li, C.; Fang, P. Highly Efficient Visible-Light-Induced Photoactivity of Z-Scheme g-C₃N₄/Ag/MoS₂ Ternary Photocatalysts for Organic Pollutant Degradation and Production of Hydrogen. *ACS Sustain. Chem. Eng.* **2017**, *5*, 1436–1445. [[CrossRef](#)]
115. Beyhaqi, A.; Zeng, Q.; Chang, S.; Wang, M.; Taghi Azimi, S.M.; Hu, C. Construction of g-C₃N₄/WO₃/MoS₂ Ternary Nanocomposite with Enhanced Charge Separation and Collection for Efficient Wastewater Treatment under Visible Light. *Chemosphere* **2020**, *247*, 125784. [[CrossRef](#)] [[PubMed](#)]
116. Pant, B.; Park, M.; Park, S.J. MoS₂/CdS/TiO₂ Ternary Composite Incorporated into Carbon Nanofibers for the Removal of Organic Pollutants from Water. *Inorg. Chem. Commun.* **2019**, *102*, 113–119. [[CrossRef](#)]
117. Shanmugam, V.; Jeyaperumal, K.S.; Mariappan, P.; Muppudathi, A.L. Fabrication of Novel g-C₃N₄ Based MoS₂ and Bi₂O₃ Nanorod Embedded Ternary Nanocomposites for Superior Photocatalytic Performance and Destruction of Bacteria. *New J. Chem.* **2020**, *44*, 13182–13194. [[CrossRef](#)]
118. Ikram, M.; Khan, M.I.; Raza, A.; Imran, M.; Ul-Hamid, A.; Ali, S. Outstanding Performance of Silver-Decorated MoS₂ Nanopetals Used as Nanocatalyst for Synthetic Dye Degradation. *Phys. E Low-Dimens. Syst. Nanostruct.* **2020**, *124*, 114246. [[CrossRef](#)]
119. Mohammed, R.; Eid, M.; Ali, M.; Abdel-moniem, S.M.; Ibrahim, H.S. Nano-Structures & Nano-Objects Reusable and Highly Stable MoS₂ Nanosheets for Photocatalytic, Sonocatalytic and Thermocatalytic Degradation of Organic Dyes: Comparative Study. *Nano-Struct. Nano-Objects* **2022**, *31*, 100900.
120. Sindhu, A.S.; Shinde, N.B.; Harish, S.; Navaneethan, M.; Eswaran, S.K. Recoverable and Reusable Visible-Light Photocatalytic Performance of CVD Grown Atomically Thin MoS₂ Films. *Chemosphere* **2022**, *287*, 132347. [[CrossRef](#)]
121. Rani, A.; Singh, K.; Sharma, P. Investigation of Visible Light Photocatalytic Degradation of Organic Dyes by MoS₂ Nanosheets Synthesized by Different Routes. *Bull. Mater. Sci.* **2022**, *45*, 63. [[CrossRef](#)]
122. Yuan, B.; Yang, L.; Yang, H.; Bai, L.; Wang, W.; Wei, D.; Liang, Y.; Chen, H. Flexible Vacancy-Mediated MoS_{2-x} Nanosheet Arrays for Solar-Driven Interfacial Water Evaporation, Photothermal-Enhanced Photodegradation, and Thermoelectric Generation. *Energy Convers. Manag.* **2022**, *252*, 115070. [[CrossRef](#)]
123. Li, H.; Shen, H.; Duan, L.; Liu, R.; Li, Q.; Zhang, Q.; Zhao, X. Enhanced Photocatalytic Activity and Synthesis of ZnO Nanorods/MoS₂ Composites. *Superlattices Microstruct.* **2018**, *117*, 336–341. [[CrossRef](#)]
124. Abinaya, R.; Archana, J.; Harish, S.; Navaneethan, M.; Ponnusamy, S.; Muthamizhchelvan, C.; Shimomura, M.; Hayakawa, Y. Ultrathin Layered MoS₂ Nanosheets with Rich Active Sites for Enhanced Visible Light Photocatalytic Activity. *RSC Adv.* **2018**, *8*, 26664–26675. [[CrossRef](#)]
125. Sabarinathan, M.; Harish, S.; Archana, J.; Navaneethan, M.; Ikeda, H.; Hayakawa, Y. Highly Efficient Visible-Light Photocatalytic Activity of MoS₂-TiO₂ Mixtures Hybrid Photocatalyst and Functional Properties. *RSC Adv.* **2017**, *7*, 24754–24763. [[CrossRef](#)]

126. Jiang, Q.; Wang, S.; Li, X.; Han, Z.; Zhao, C.; Di, T.; Liu, S.; Cheng, Z. Controllable Growth of MoS₂ nanosheets on TiO₂ burst Nanotubes and Their Photocatalytic Activity. *RSC Adv.* **2020**, *10*, 40904–40915. [[CrossRef](#)]
127. Tama, A.M.; Das, S.; Dutta, S.; Bhuyan, M.D.I.; Islam, M.N.; Basith, M.A. MoS₂ Nanosheet Incorporated α -Fe₂O₃/ZnO Nanocomposite with Enhanced Photocatalytic Dye Degradation and Hydrogen Production Ability. *RSC Adv.* **2019**, *9*, 40357–40367. [[CrossRef](#)] [[PubMed](#)]
128. Sharma, M.; Mohapatra, P.K.; Bahadur, D. Improved Photocatalytic Degradation of Organic Dye Using Ag₃PO₄/MoS₂ Nanocomposite. *Front. Mater. Sci.* **2017**, *11*, 366–374. [[CrossRef](#)]
129. Raja, V.R.; Rosaline, D.R.; Suganthi, A.; Rajarajan, M. Facile Fabrication of PbS/ MoS₂ Nanocomposite Photocatalyst with Efficient Photocatalytic Activity under Visible Light. *Solid State Sci.* **2017**, *67*, 99–108. [[CrossRef](#)]
130. Zhang, S.; Wang, L.; Liu, C.; Luo, J.; Crittenden, J.; Liu, X.; Cai, T.; Yuan, J.; Pei, Y.; Liu, Y. Photocatalytic Wastewater Purification with Simultaneous Hydrogen Production Using MoS₂ QD-Decorated Hierarchical Assembly of ZnIn₂S₄ on Reduced Graphene Oxide Photocatalyst. *Water Res.* **2017**, *121*, 11–19. [[CrossRef](#)]
131. Rani, A.; Singh, K.; Patel, A.S.; Chakraborti, A.; Kumar, S.; Ghosh, K.; Sharma, P. Visible Light Driven Photocatalysis of Organic Dyes Using SnO₂ Decorated MoS₂ Nanocomposites. *Chem. Phys. Lett.* **2020**, *738*, 136874. [[CrossRef](#)]
132. Lu, Y.; Xu, L.; Liu, C. Magnetically Separable and Recyclable Photocatalyst MoS₂-SrFe₁₂O₁₉ with p-n Heterojunction: Fabrication, Characterization, and Photocatalytic Mechanism. *Appl. Organomet. Chem.* **2020**, *34*, 1–15. [[CrossRef](#)]
133. Gawari, D.; Pandit, V.; Jawale, N.; Kamble, P. Proceedings Layered MoS₂ for Photocatalytic Dye Degradation. *Mater. Today Proc.* **2022**, *53*, 10–14. [[CrossRef](#)]
134. Jia, Y.; Ma, H.; Liu, C. Au Nanoparticles Enhanced Z-Scheme Au-CoFe₂O₄/MoS₂ Visible Light Photocatalyst with Magnetic Retrievalability. *Appl. Surf. Sci.* **2019**, *463*, 854–862. [[CrossRef](#)]
135. Gao, J.; Hu, J.; Wang, Y.; Zheng, L.; He, G.; Deng, J.; Liu, M.; Li, Y.; Liu, Y.; Zhou, H. Fabrication of Z-Scheme TiO₂/SnS₂/MoS₂ Ternary Heterojunction Arrays for Enhanced Photocatalytic and Photoelectrochemical Performance under Visible Light. *J. Solid State Chem.* **2022**, *307*, 122737. [[CrossRef](#)]
136. Khaing, K.K.; Yin, D.; Ouyang, Y.; Xiao, S.; Liu, B.; Deng, L.; Li, L.; Guo, X.; Wang, J.; Liu, J.; et al. Fabrication of 2D–2D Heterojunction Catalyst with Covalent Organic Framework (COF) and MoS₂ for Highly Efficient Photocatalytic Degradation of Organic Pollutants. *Inorg. Chem.* **2020**, *59*, 6942–6952. [[CrossRef](#)]
137. Lv, H.; Liu, Y.; Tang, H.; Zhang, P.; Wang, J. Synergetic Effect of MoS₂ and Graphene as Cocatalysts for Enhanced Photocatalytic Activity of BiPO₄ Nanoparticles. *Appl. Surf. Sci.* **2017**, *425*, 100–106. [[CrossRef](#)]
138. Zhang, B.; Shi, H.; Hu, X.; Wang, Y.; Liu, E.; Fan, J. A Novel S-Scheme MoS₂/CdIn₂S₄ Flower-like Heterojunctions with Enhanced Photocatalytic Degradation and H₂ Evolution Activity. *J. Phys. D Appl. Phys.* **2020**, *53*, 205101. [[CrossRef](#)]
139. Ren, B.; Shen, W.; Li, L.; Wu, S.; Wang, W. 3D CoFe₂O₄ Nanorod/Flower-like MoS₂ Nanosheet Heterojunctions as Recyclable Visible Light-Driven Photocatalysts for the Degradation of Organic Dyes. *Appl. Surf. Sci.* **2018**, *447*, 711–723. [[CrossRef](#)]
140. Lu, M.; Xiao, X.; Wang, Y.; Chen, J. Construction of Novel BiOIO₃/MoS₂ 2D/2D Heterostructures with Enhanced Photocatalytic Activity. *J. Alloys Compd.* **2020**, *831*, 154789. [[CrossRef](#)]
141. Rathnasamy, R.; Santhanam, M.; Alagan, V. Anchoring of ZnO Nanoparticles on Exfoliated MoS₂ Nanosheets for Enhanced Photocatalytic Decolorization of Methyl Red Dye. *Mater. Sci. Semicond. Process.* **2018**, *85*, 59–67. [[CrossRef](#)]
142. Talukdar, K.; Saravanakumar, K.; Kim, Y.; Fayyaz, A.; Kim, G.; Yoon, Y.; Park, C.M. Rational Construction of CeO₂-ZrO₂@MoS₂ Hybrid Nanoflowers for Enhanced Sonophotocatalytic Degradation of Naproxen: Mechanisms and Degradation Pathways. *Compos. Part B Eng.* **2021**, *215*, 108780. [[CrossRef](#)]
143. Ji, R.; Zhu, Z.; Ma, W.; Tang, X.; Liu, Y.; Huo, P. A Heterojunction Photocatalyst Constructed by the Modification of 2D-CeO₂ on 2D-MoS₂ Nanosheets with Enhanced Degrading Activity. *Catal. Sci. Technol.* **2020**, *10*, 788–800. [[CrossRef](#)]
144. Zhang, X.; Xia, M.; Wang, F.; Lei, W. Cu₂O/ MoS₂ Composites: A Novel Photocatalyst for Photocatalytic Degradation of Organic Dyes under Visible Light. *Ionics* **2020**, *26*, 6359–6369. [[CrossRef](#)]
145. Fu, Y.; Li, Z.; Liu, Q.; Yang, X.; Tang, H. Construction of Carbon Nitride and MoS₂ Quantum Dot 2D/0D Hybrid Photocatalyst: Direct Z-Scheme Mechanism for Improved Photocatalytic Activity. *Cuihua Xuebao/Chin. J. Catal.* **2017**, *38*, 2160–2170. [[CrossRef](#)]
146. Feng, H.; Zhou, W.; Zhang, X.; Zhang, S.; Liu, B.; Zhen, D. Synthesis of Z-Scheme Mn-CdS/ MoS₂/TiO₂ Ternary Photocatalysts for High-Efficiency Sunlight-Driven Photocatalysis. *Adv. Compos. Lett.* **2019**, *28*, 1–10. [[CrossRef](#)]